Applied Energy 352 (2023) 121885

Contents lists available at ScienceDirect

Applied Energy

journal homepage: www.elsevier.com/locate/apenergy

Pioneering sustainable power: Harnessing material innovations in double stage segmented thermoelectric generators for optimal 4E performance

Hisham Alghamdi [a], Chika Maduabuchi [b,c,*], Kingsley Okoli [c,d], Abdullah Albaker [e], Emad Makki [f], Mohammed Alghassab [g,**], Mohammad Alobaid [h,***], Mohammad Alkhedher [i]

[a] Electrical Engineering Department, College of Engineering, Najran University, Najran 55461, Saudi Arabia
[b] Department of Nuclear Science and Engineering, Massachusetts Institute of Technology, Cambridge, MA, USA
[c] Artificial Intelligence Laboratory, University of Nigeria Nsukka, Nsukka 410001, Enugu, Nigeria
[d] Department of Computer Science and Knowledge Discovery, Saint Petersburg Electrotechnical University LETI, Saint Petersburg 197022, Russia
[e] Department of Electrical Engineering, College of Engineering, University of Ha'il, Ha'il 81451, Saudi Arabia
[f] Department of Mechanical Engineering, College of Engineering and Islamic Architecture, Umm Al-Qura University, Makkah 24382, Saudi Arabia
[g] Electrical Engineering Department, College of Engineering, Shaqra University, Riyadh 11911, Saudi Arabia
[h] Department of Mechanical and Industrial Engineering, College of Engineering, Majmaah University, Al-Majmaah 11952, Saudi Arabia
[i] Department of Mechanical and Industrial Engineering, Abu Dhabi University, Abu Dhabi 59911, United Arab Emirates

HIGHLIGHTS

- Optimized DSSTEGs for efficient solar energy conversion.
- Skutterudite content at 6.17% maximizes DSSTEG performance.
- CO_2 savings of 23.78 kgyr^{-1} achieved with optimal parameters.
- High output power of 50.08 W at optimal skutterudite content.
- Balanced cost-effectiveness with $0.05 per watt output.

ARTICLE INFO

Keywords:
Performance analysis
Absorbed solar flux
Design optimization
Energy sustainability
Segmented thermoelectric

ABSTRACT

This study presents groundbreaking advancements in sustainable power through a comprehensive exploration of double-stage segmented thermoelectric generators (DSSTEGs) optimized for efficient solar energy conversion. Specifically comparing DSSTEGs with other solar thermoelectric generator (STEG) configurations through geometry parametric optimization, we elucidate the intricate interplay between material properties and design parameters using a finite element method-driven numerical approach. The focus is on achieving 4E optimization (energy, exergy, environmental, and economic factors). Our results demonstrate that a skutterudite content of 6.17% maximizes DSSTEG performance, showcasing its superiority over conventional STEGs. The optimized DSSTEG excels with remarkable CO_2 savings of 23.78 kgyr^{-1} and an impressive high output power of 50.08 W at the optimal skutterudite content. Moreover, the DSSTEG design demonstrates a balanced cost-effectiveness with an outstanding $0.05 per watt output, surpassing conventional STEGs' cost-efficiency. These findings offer a pragmatic framework for integrating innovative materials and optimized designs in concentrated solar energy applications, signifying a significant stride in the field of thermoelectric generators. The pivotal role of materials and design in defining and optimizing performance for enhanced solar energy conversion is highlighted, propelling the path towards a more sustainable and efficient energy future.

* Corresponding author at: Department of Nuclear Science and Engineering, Massachusetts Institute of Technology, Cambridge, MA, USA.
** Corresponding author.
*** Corresponding author.
E-mail addresses: chika691@mit.edu, chika.maduabuchi.191341@unn.edu.ng (C. Maduabuchi), malghassab@su.edu.sa (M. Alghassab), m.alobaid@mu.edu.sa (M. Alobaid).

https://doi.org/10.1016/j.apenergy.2023.121885
Received 11 June 2023; Received in revised form 22 July 2023; Accepted 2 September 2023
Available online 19 September 2023
0306-2619/

1. Introduction

In the face of escalating global energy demands and mounting concerns over climate change, the urgency of discovering efficient, sustainable, and environmentally responsible power generation technologies has never been more pressing. Segmented Thermoelectric Generators (STEGs), specifically designed for concentrated solar energy conversion, stand out as a beacon of hope in this regard. These innovative devices harness the power of the thermoelectric effect [1], converting the sun's abundant and renewable energy directly into electricity [2]. STEGs represent a leap forward from traditional TEGs by employing a stacked configuration of thermoelectric materials, thereby managing a more extensive temperature gradient range to boost efficiency and power output [3]. Despite the undeniable potential and growing interest in STEGs, a comprehensive exploration of their energy, exergy, environmental, and economic (4E) performance remains surprisingly scarce. Addressing this oversight, the present study offers a comprehensive analysis and optimization of a double-stage STEG, shining a light on both the promising capabilities and possible constraints of this technology in the realm of concentrated solar energy conversion.

Since the initial conception of STEG technology by Soviet researcher Ioffe and colleagues [4], numerous research endeavors [5] have been dedicated to evolving this technology towards practical viability. This body of work has produced some significant findings. For instance, Tian et al., [6] demonstrated through thermal, exergy, and economic analyses that the dollar per watt ratio of a segmented annular TEG was superior to its traditional counterpart under fixed hot and cold junction temperatures. Similarly, Ge et al., [7] achieved a remarkable 24.39% increase in output power from an optimized STEG, designed for waste heat recovery, under uniform junction temperatures. In an innovative application of evolutionary computation and finite element methodologies, Chen and Chou [8] succeeded in optimizing STEG geometry parameters to bolster power and efficiency by 21.94% and 14.05% respectively. Furthermore, Wen et al., [9] reported maximum power and efficiency under matched load conditions for a tri-STEG with an annular shape, while Aljaghtham and Celik [10] proposed a unileg TEG design to enhance the thermal reliability of STEGs.

In the quest for harnessing the full potential of TEG technology, the concept of double-staging the thermoelectric segments has been extensively explored, giving birth to the Double-Stage Thermoelectric Generator (DSTEG). This ingenious strategy seeks to amplify power output and conversion efficiency by extending the operable temperature range of the device [11]. By providing optimal temperature conditions for each stage, DSTEG leverages the unique properties of thermoelectric materials across different temperature ranges, achieving unmatched performance under the high-temperature gradients characteristic of concentrated solar applications [12].

This section delves into some of the cutting-edge developments in DSTEG technology. One innovative approach undertaken by Sun et al., [13] combined the finite element method with genetic algorithms to optimize the geometric parameters of a DSTEG. This design utilized skutterudite in the upper stage and bismuth-telluride in the lower stage, focusing on optimizing the specific power and entropy generation. Similarly, Yin et al., [14] employed a one-dimensional numerical model to quantify the multi-parameter uncertainty inherent in temperature-dependent materials in three-stage thermoelectric couples. This sophisticated analysis yielded an impressive optimal efficiency of 18.06% at an optimal height of 3 mm with a fixed temperature difference of 500 K.

In another ground-breaking effort, Zhang et al., [15] used finite time thermodynamics in combination with a one-dimensional model and Latin hypercube sampling to investigate a DSTEG operating under a fixed temperature gradient. Broadening the horizons of DSTEG applications, researchers have successfully incorporated this technology into hybrid systems, such as high-temperature proton exchange fuel cells [16] and photovoltaic modules [17]. These pioneering studies, considering factors like the Thomson effect, underscore the versatility and potential of DSTEGs in a range of energy conversion contexts.

Moreover, another approach to boost the performance of TEGs involves varying the geometry of the thermoelectric leg. While this technique has been largely confined to single-stage designs so far, it has shown remarkable potential in enhancing the efficiency and power output of the device. For instance, Sahoo and Karana [18] developed a one-dimensional model for an extended-tapering STEG, which exhibited a 16% exergy efficiency under fixed temperature conditions.

Exploring further, Mohammad Siddique et al., [19] contemplated diverse leg geometries and nanostructured TE materials to elevate the thermal efficiency of TEGs. They employed a numerical two-dimensional method, and the designed system displayed a significant improvement in thermal efficiency, raising it from 7.3% to 8.7%, given hot and cold junction temperatures of 500 K and 300 K, respectively.

Interestingly, Zhang et al., [20] experimentally demonstrated that the fusion of optimal leg geometries could yield 66% - 98% greater power density compared to traditional TE legs, attributable to the lesser mass of the variable area legs. Reinforcing this view, Mohammad Siddique et al., [21] substantiated through experiments that trapezoidal-shaped TE pellets generated 1.24 and 1.5 times more voltage and power, respectively, than the conventional rectangular-shaped prototype under specific temperature conditions. They also highlighted the significance of boundary conditions in determining the optimal leg shape.

Meanwhile, Weng et al., [22] ventured into the realm of variable angle leg annular TEGs, conducting a performance analysis under varying boundary conditions using a three-dimensional numerical model. They concluded that, under a constant hot junction heat flux and cold junction temperature, the system's output performance could be amplified by a factor of 35%, albeit at the cost of 30% higher thermal stress in the TE cavity. This indicates a crucial trade-off to consider in design optimization.

From an exhaustive review of existing literature, it is apparent that while thermoelectric generators (TEGs) have undergone considerable advancements, there remains a palpable dearth in several critical areas, which opens avenues for novel contributions:

1. There is a notable scarcity in the literature regarding an integrated analysis of double-stage TEGs that utilize segmented thermoelectric (TE) materials with trapezoidal legs, with an emphasis on a holistic evaluation encompassing energy, exergy, environmental, and economic (4E) aspects.
2. In addition, there is limited exploration into how design parameters, particularly TE leg geometry and material composition (e.g., skutterudite content), impact critical performance metrics like power output, exergy efficiency, CO_2 savings, and cost-effectiveness.
3. Most studies on high-temperature TEGs focus on conventional designs and fail to investigate innovative structures tailored for concentrated solar energy applications, such as the double-stage segmented variable area leg thermoelectric generator (DSSVAL TEG).

Addressing these gaps, our study introduces several ground-breaking contributions that are pivotal to the physics of materials, particularly in the realm of thermal energy conversion:

1. We present a cutting-edge DSSVAL TEG design tailored for concentrated solar energy applications. This innovation is centered around the novel integration of trapezoidal-legged segmented TE materials, and it represents a leap in the development of high-temperature TEGs.
2. At the heart of this study is an unparalleled 4E parametric optimization analysis, which dissects the interplay between material properties, geometric intricacies, and thermal characteristics. This

serves not only as a holistic evaluation but also as a foray into the underlying physics governing the system's performance.

3. Our investigation pioneers the scrutiny of specific design parameters, such as TE leg geometry and skutterudite content, and their influence on key performance indicators. This contributes a pioneering framework that intertwines materials physics with design optimization for DSSVAL TEGs.
4. Collectively, this research provides a comprehensive and scientifically rigorous blueprint for the advancement and deployment of DSSVAL TEGs in concentrated solar energy applications. This stands as a seminal contribution in bridging crucial gaps in the current literature, and it holds immense implications for sustainable energy solutions through the lens of materials physics.

We believe that this study's focused inquiry into the physics of materials within the context of thermoelectric energy conversion, coupled with its innovative approach to design optimization, aligns with the ethos of Materials Today Physics and adds significant value to its scholarly discourse.

2. Methodology

This section provides a systematic overview of the Double-Stage Thermoelectric Generator (DSSTEG) system analyzed in this study. The DSSTEG, illustrated in Fig. 1, is constructed from two HT 6–12-40 modules consisting of 127 thermocouples, electrically connected in series and thermally in parallel. The modules have surface dimensions of 40 mm × 40 mm. Detailed dimensions of the thermoelectric cell are furnished within the figure. (See Fig. 1.)

The temperature sensitive behaviour of the semiconductors utilized in this study are provided in Fig. 2.

2.1. Thermoelectric field equations

The three-dimensional energy equation is given by [23]:

$$\rho C_p \frac{\partial T}{\partial t} + \nabla . \vec{q} = \dot{q} \tag{1}$$

where ρ is the density, C_p is the specific heat capacity, T is the temperature, $\vec{q}$ is the heat density vector, and $\dot{q}$ is the heat flux vector.

Meanwhile the electrical current conservation equation is given as [24]:

$$\nabla . \left(\vec{J} + \frac{\partial \vec{D}}{\partial t} \right) = 0 \tag{2}$$

where $\vec{J}$ is the current density vector and $\vec{D}$ is the electric displacement vector.

$\vec{J}$ is further defined as [25]:

$$\vec{J} = \sigma \left(\vec{E} - S \nabla T \right) \tag{3}$$

where $\vec{E}$ is the electric field intensity vector, S is the Seebeck coefficient, and σ is the electrical conductivity, given as the reciprocal of the electrical resistivity of the thermoelectric materials.

$\vec{E}$, $\dot{q}$ and $\vec{q}$ are given as [26]:

$$\vec{E} = -\nabla V \tag{4}$$

$$\dot{q} = \vec{J} . \vec{E} \tag{5}$$

$$\vec{q} = -k \nabla T + S \vec{J} T \tag{6}$$

where V is the electrical scalar potential, k is the thermal conductivity, and S is the Seebeck coefficient.

Coupling these field equations, we get the thermoelectric field equation as:

$$\rho C_p \frac{\partial T}{\partial t} + \nabla . (-k \nabla T - ST(\sigma \nabla V + S \nabla T)) = (-\sigma \nabla V - S\sigma \nabla T) . (-\nabla V) \tag{7}$$

Assuming steady-state conditions, the steady coupled thermal-electrical equation becomes

$$\nabla . (-k \nabla T - ST(\sigma \nabla V + S \nabla T)) = (-\sigma \nabla V - S\sigma \nabla T) . (-\nabla V) \tag{8}$$

2.2. Performance equations

Subsequently, the power output is obtained under maximum power transfer theory as [27]:

$$P_{TE} = \frac{(S \Delta T)^2}{4R} \tag{9}$$

where R is the internal electrical resistance of the thermoelectric semiconductor, and ΔT is the temperature gradient across the TEG's junctions.

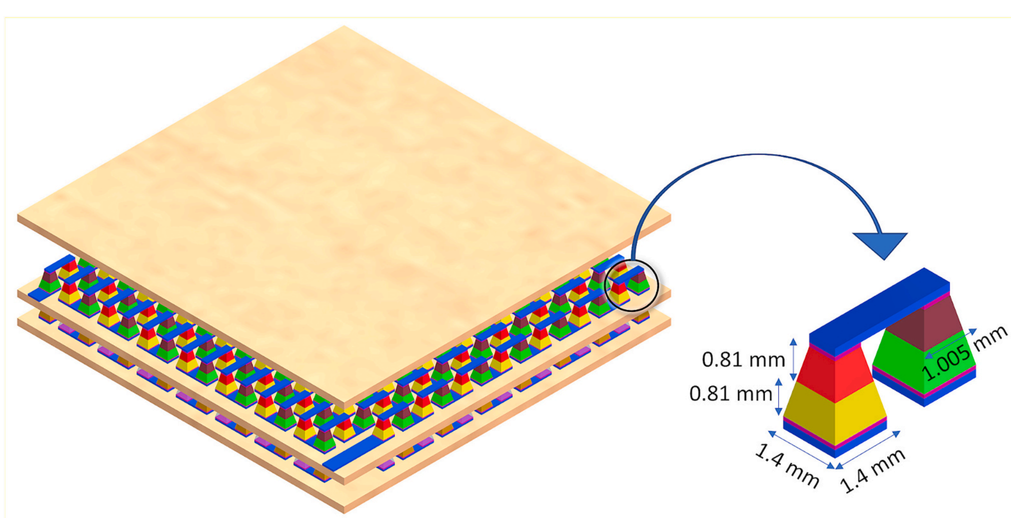

Fig. 1. Three-dimensional model of the DSSTEG with trapezoidal-shaped pellets.

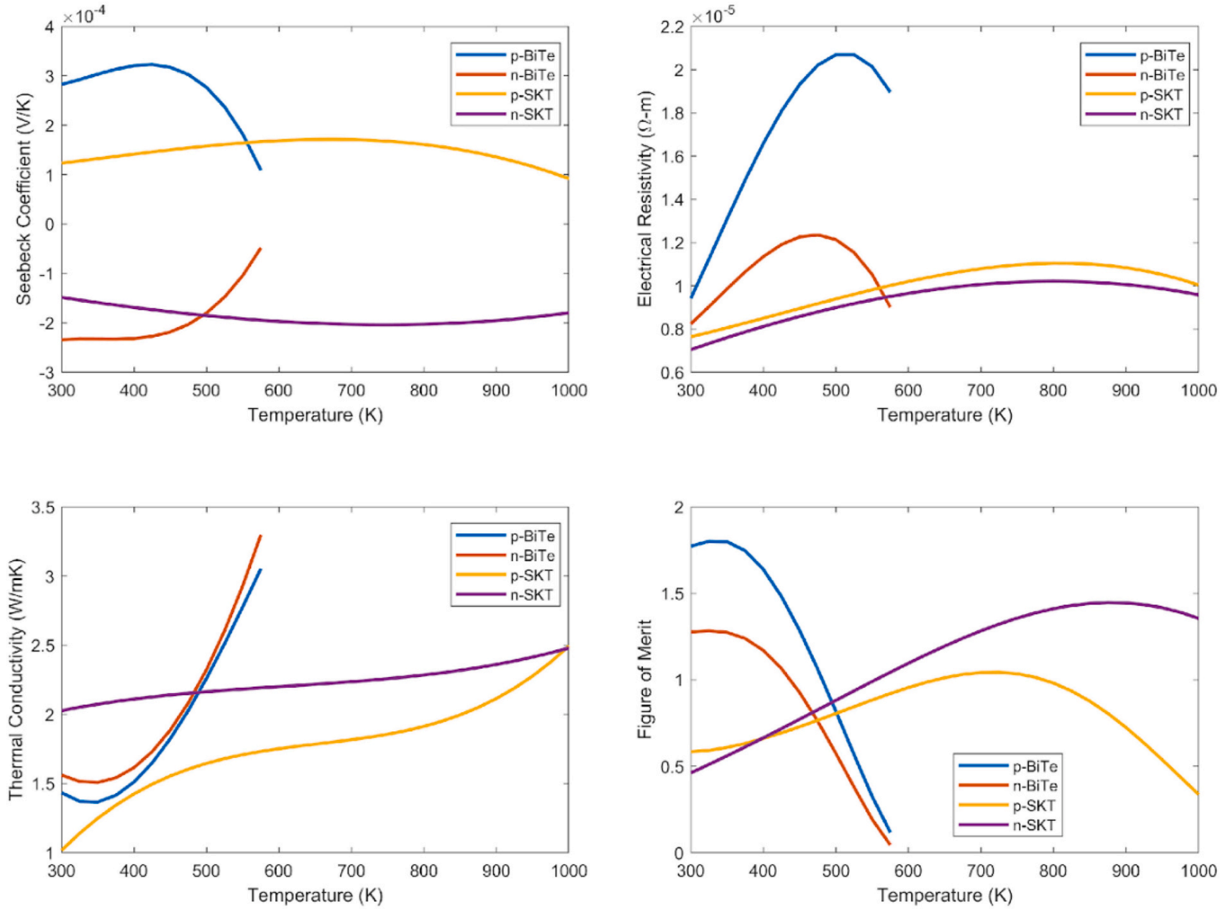

Fig. 2. Plot of material properties against temperature

Then, the exergy efficiency is obtained as [28]:

$$\eta_{ex} = \frac{P_{TE}}{\Psi Q_{in}} \tag{10}$$

where Ψ is the Petela's constant [29] expressed as: $\Psi = \left[1 - \frac{4}{3}\left(\frac{T_a}{T_s}\right) + \frac{1}{3}\left(\frac{T_a}{T_s}\right)^4\right]$, for T_a as the temperature of the surroundings (295.15 K) and T_s as the Sun's black body temperature (5778 K).

A robust method of examining the environmental impact of a technology is by determining its carbon (iv) oxide emissions (CO_2) during operation [30]. Besides, the objective of adapting renewables is to minimize CO_2 emissions, hence, this paper calculates the amount of CO_2 emissions savings per year for the TSTEG assuming the worst-case scenario of a gas power plant [31]:

$$CO_2 = P_y CEI \tag{11}$$

where CEI is the CO_2 emission intensity (0.475 kgCO_2eq/kWh, [53]), and P_y is the yearly power generation in kWh assuming 365 days of operation and an average sunshine hour of 10 h [32].

Finally, the economic viability of a technology is of utmost importance to investors when making financial decisions [33]. Therefore, this work calculates the dollar per watt generated by the TSTEG (DPW) as follows [34]:

$$DPW = \frac{1}{P_{TE}} \times \sum_{i=1}^{N} (C_i V_i) \tag{12}$$

where V_i is the volume occupied by the thermoelectric elements in mm^3 and C_i is the volumetric cost of the materials in \$/mm^3 reported in ref. [35].

2.3. Boundary conditions

The boundary conditions used to define the virtual model of the Double-Stage Thermoelectric Generator (DSSTEG) are as follows:

1. **Hot Side Boundary Condition**: Unless otherwise stated, a constant heat flux of 10 kWm^{-2} is applied to the hot side of the DSSTEG, simulating the thermal energy input. This is representative of the heat source, such as waste heat or solar radiation, depending on the application.
2. **Cold Side Boundary Condition**: On the cold side of the DSSTEG, unless otherwise stated, a convective heat transfer boundary condition is applied with a heat transfer coefficient of 1 kWm^{-2} K^{-1}. This simulates the heat dissipation to the ambient or a heat sink, and it is crucial for maintaining a temperature gradient across the thermoelectric materials.
3. **Electrical Boundary Conditions**: For the electrical analysis, the DSSTEG's *n*-type semiconductor is set to ground potential, representing the electrical reference point. The *p*-type semiconductor has a floating potential, and the terminal voltage across the thermoelectric couple is dynamically determined based on the Seebeck effect and the current flowing through the device.
4. **Thermoelectric Material Properties**: The properties of the thermoelectric materials used in the DSSTEG, such as Seebeck coefficient, electrical conductivity, and thermal conductivity, are defined based on experimental data obtained from the literature values [8]. These properties are temperature-dependent and are defined accurately for precise simulation results.

5. **External Load**: An external electrical load is connected across the terminals of the DSSTEG to draw the electric power generated. The load is assumed fixed and is equal to the intrinsic electrical resistance of the thermoelectric semiconductors.
6. **Geometry and Dimensions**: The geometry and dimensions of the DSSTEG, such as the thickness and area of the thermoelectric materials, the length of the legs, and the contact area with the heat source and sink, are precisely defined to represent the physical prototype accurately.

These boundary conditions and parameters are essential in creating an accurate virtual model of the DSSTEG for simulations and analyses of its performance under varying operating conditions.

2.4. Validation and comparative analysis

In this study, the reliability and accuracy of the numerical optimization method employed are scrutinized through a series of validation and verification exercises. These exercises ensure that the optimization insights acquired are firmly grounded in both empirical evidence and theoretical consistency.

Firstly, a benchmark comparison is made between the results obtained in this work and those documented in prior numerical and experimental studies, as a way to standardize the optimization method. Such benchmarking practices have been widely adopted in literature [36] to validate and corroborate the insights from optimization studies. Specifically, the numerical method in this study is deployed to recreate both experimental and theoretical results from preceding papers focusing on concentrating solar thermoelectric technology. Fig. 3 illustrates this comparison.

In addition to the comparative benchmarking, a mesh sensitivity analysis serves as an auxiliary tool for verifying the numerical results. This involves investigating the optimal element size at which the system's output parameters, such as power output converge. The mesh sensitivity analysis is a robust and widely acknowledged approach in numerical modeling, as endorsed by numerous scholars [39]. For this study, the ANSYS parametric mesh convergence toolbox facilitates the mesh sensitivity analysis. Table 1 exhibits the results of this analysis, detailing the grid points and the corresponding power output at various mesh densities.

Through these comprehensive validation and verification procedures, this study ensures the reliability and accuracy of the numerical optimization method and the results derived from it.

2.5. Selection of cold side heat transfer coefficient

A critical parameter that significantly influences the performance of our Double Stage Segmented Thermoelectric Generator (DSSTEG) is the cold side heat transfer coefficient (HTC). The HTC dictates the rate at which heat is rejected from the system, hence directly impacting the thermal gradients across the thermoelectric (TE) legs, and in turn, the power output and efficiency of the system.

The cold side HTC of 1 kW/m^{2}K, equivalent to 1000 W/m^{2}K, used in this study corresponds to a scenario where forced convection cooling is employed, such as utilizing a pump for circulating a coolant like distilled water. This value was not arbitrarily chosen; it is founded on heat transfer theory and corresponds to the range of HTCs that can be realistically achieved under such conditions. The precise value can be computed using appropriate heat transfer correlations. For instance, in the case of turbulent flow, the Dittus-Boelter equation can be used, and for laminar flow or situations where the fluid properties change significantly with temperature, the Sieder-Tate correlation can be employed.

To account for a variety of cooling conditions that might be encountered in practical applications, a sensitivity analysis was conducted by varying the cold side HTC between 1 kW/m^{2}K and 4 kW/m^{2}K. This analysis captured the range of HTCs obtainable under diverse circumstances, considering variables such as the coolant type, flow rate, system design, and environmental parameters.

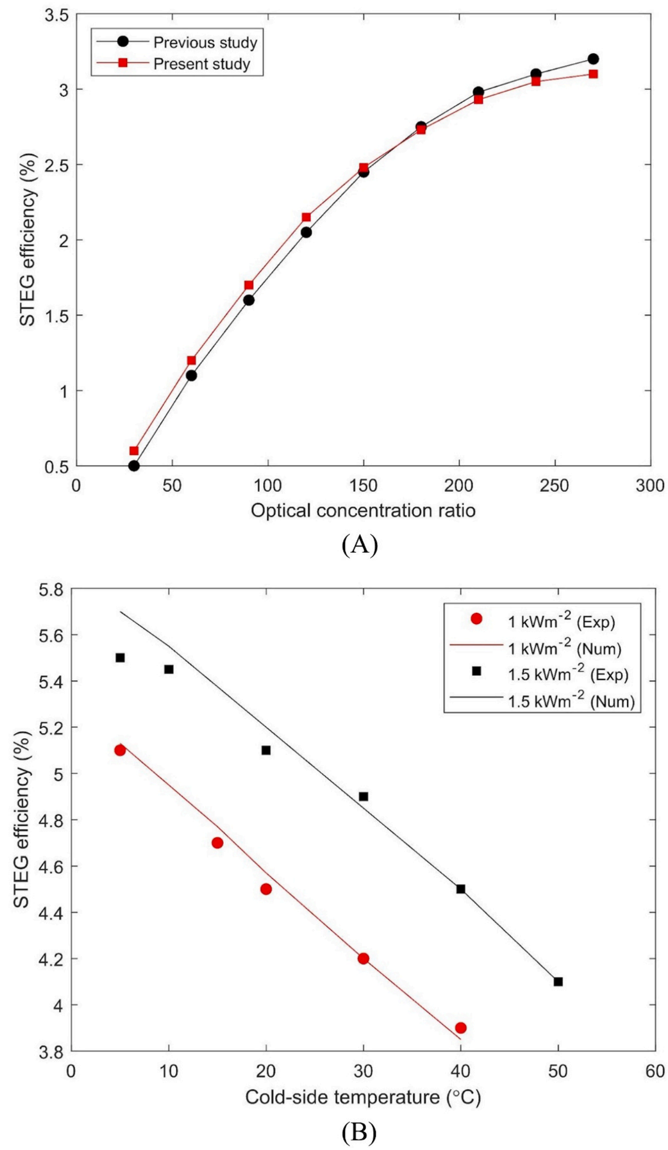

Fig. 3. (A) Juxtaposition of the numerical findings from this study with the experimental data from a preceding study on concentrating solar thermoelectric technology [37]. (B) Alignment of the numerical outcomes with the theoretical results of a prior study on concentrating solar thermoelectric technology [38].

Table 1
Mesh Sensitivity Study Outcomes – A display of grid points alongside the corresponding power output (W) at divergent mesh densities.

S/N	Grid Points	Power Output (W)
1	16,437	5.139216
2	30,893	5.139038
3	79,336	5.138978
4	212,573	5.139340
5	513,473	5.139340

It is crucial to note that the actual HTC in real-world scenarios can vary based on numerous factors, and the chosen value in this study is primarily intended for comparative analysis and understanding the sensitivity of the DSSTEG system's performance to this parameter.

This study underscores the need for a comprehensive understanding of heat transfer dynamics in the design and operation of thermoelectric generators. Future work should involve more detailed investigations of cooling systems' configurations and operating conditions to determine the most effective and efficient methods of heat rejection. Such studies will further refine our understanding of these systems, thereby contributing to the development of more efficient and versatile thermoelectric energy conversion technologies.

The selection of a cold side HTC value of 1 $kWm^{-2} K^{-1}$ as the base case in our study served the purpose of conducting a comprehensive sensitivity analysis and exploring the DSSTEG's performance under challenging heat dissipation conditions. This choice was made to provide valuable insights into the system's sensitivity to variations in the HTC, emphasizing its potential in sustainable energy conversion scenarios. Nonetheless, we acknowledge that the real-world selection of the cold side HTC requires a more detailed engineering analysis, taking into account specific operating conditions and design considerations.

3. Results and discussion

This section depicts and discusses the results obtained from the 4E (energy, exergy, environment, and economic) performance optimization of the DSSTEG for sustainable power generation from concentrated solar energy. The combined impacts of concentrated solar energy and convective heat transfer coefficient as well as the geometry parameters like the semiconductor height, cross-sectional area and skutterudite amount are comprehensively investigated. The performance parameters computed include the power output (energy), exergy efficiency (exergy), CO_2 savings (environment), and dollar per watts (economic). The geometry parameters are optimized by varying them through a parametric study initiated by the ANSYS numerical software actively coupled with the computer aided design software.

3.1. Combined effects of solar flux and cooling heat transfer coefficient

In this study, we adopt a strategic methodology for determining the optimal upper limit of the concentrated solar irradiance for the operation of the skutterudite thermoelectric generator (STEG). Our approach hinges on a comprehensive sensitivity analysis and the considerations imposed by the unique thermoelectric properties of our selected material—bismuth-telluride and skutterudite—and the device's specific geometric parameters.

Initially, an increase in the hot junction heat flux augments the absorbed solar energy at the device's hot junction, intensifying the temperature gradient between the hot and cold junctions under a specific cooling condition. However, considering our device's geometric conditions (skutterudite content, leg height, and leg area), there exists an optimal heat flux, beyond which the device's output power begins to decline precipitously. This phenomenon results from the temperature-dependent behavior of the thermoelectric semiconductor at varying heat flux applications.

Our rigorous sensitivity analysis, in consideration of the device's geometry parameters and cooling conditions, revealed that the optimal heat flux for maximizing the power output of the STEG was at 77 kW/m^2. While the heat flux could exceed this point, it would negatively impact the power output due to the deterioration of the device's thermoelectric properties.

However, it is worth noting that altering the geometric parameters of the thermoelectric semiconductor, such as reducing the thermoelectric height, could potentially extend the heat flux beyond this point. The resultant changes in the thermal conductance of the thermoelectric semiconductor would lead to a readjustment of the thermal gradient, which could facilitate an optimal power output at higher heat flux levels. We have thoroughly explored these parameters in our power-leg height-heat flux plots, providing a comprehensive illustration of this complex interplay.

By incorporating this methodology in our research, we have ensured that our STEG operates under the most advantageous conditions, maximizing its power output and efficiency, and ultimately enhancing its viability in renewable energy applications.

The obtained results in Fig. 4 indicates that the DSSTEG system achieved its optimum output power of 13.66 W at an absorbed solar flux of 77 kWm^{-2}, coupled with a heat transfer coefficient of 4 $kWm^{-2} K^{-1}$. On the other hand, the system exhibited the lowest power output of 0.76 W at a minimum absorbed solar flux of 10 kWm^{-2}, which was consistent across all heat transfer coefficients. These suggest that the DSSTEG's power generation capacity is highly influenced by the intensity of the absorbed solar flux, with higher flux levels resulting in increased output power. Additionally, a higher heat transfer coefficient facilitates better heat dissipation, leading to improved power generation. The analysis reveals that the TEG system achieved its optimum exergy efficiency of 9.68% when the absorbed solar flux was 57.85 kWm^{-2} and the heat transfer coefficient was 4 $kWm^{-2} K^{-1}$. Conversely, the lowest exergy efficiency of 3.50% was observed at the minimum absorbed solar flux of 10 kWm^{-2}, regardless of the heat transfer coefficient. These results indicate that the exergy efficiency of the TEG is influenced by both the absorbed solar flux and the heat transfer coefficient. Higher absorbed solar flux levels contribute to increased thermal energy availability, resulting in improved exergy efficiency. Furthermore, a higher heat transfer coefficient facilitates more efficient heat transfer. The analysis also examines the yearly CO_2 savings achieved by the TEG system. It is observed that the maximum CO_2 savings of 6.49 $kgyr^{-1}$ is attained when the absorbed solar flux is 77 kWm^{-2} and the heat transfer coefficient is 4 $kWm^{-2} K^{-1}$. This indicates that the system, at its optimal operating conditions, can contribute significantly to reducing CO_2 emissions. Conversely, the least CO_2 savings of 0.36 $kgyr^{-1}$ are obtained when the absorbed solar flux is 10 kWm^{-2}, irrespective of the heat transfer coefficient. The metric of dollars per watts provides an economic perspective on the TEG system's performance. The study reveals that the optimum dollars per watt value of 0.20 $\$W^{-1}$ is achieved when the absorbed solar flux is 53.07 kWm^{-2} and the heat transfer coefficient is 4 $kWm^{-2} K^{-1}$. This implies that the system is cost-effective and efficient in terms of the amount of electrical power generated relative to the investment made. However, further analysis is necessary to assess the overall economic viability of the TEG system. The results demonstrate the significant impact of absorbed solar flux and cooling heat transfer coefficient on the performance of the double stage segmented thermoelectric generator. The findings provide insights into the optimal operating conditions for maximizing output power, exergy efficiency, CO_2 savings, and cost-effectiveness. This knowledge can guide the design and optimization of similar TEG systems, enhancing their overall performance and contributing to sustainable and efficient solar energy conversion.

From Fig. 5 above, the maximum output power achieved by the DSSTEG system is 8.18 W, which occurs when the cooling heat transfer coefficient is 4 $kWm^{-2} K^{-1}$ and the absorbed solar flux is 40 kWm^{-2}. This indicates that under these conditions, the system can effectively convert solar energy into electrical power. On the other hand, the minimum output power obtained is 0.73 W, which occurs when the cooling heat transfer coefficient is 0.5 $kWm^{-2} K^{-1}$ and the absorbed solar flux is 10 kWm^{-2}. This combination results in the lowest power generation capability of the DSSTEG system. The exergy efficiency of the DSSTEG system is found to be 9.03% at the optimal cooling heat transfer coefficient of 4 $kWm^{-2} K^{-1}$ and absorbed solar flux of 40 kWm^{-2}. This indicates that the system can efficiently convert concentrated solar energy into useful work. Conversely, the minimum exergy efficiency of 3.37% is observed when the cooling heat transfer coefficient is 0.5 $kWm^{-2} K^{-1}$ and the absorbed solar flux is 10 kWm^{-2}. This combination leads to a less efficient conversion of solar energy into useful work. The analysis also evaluates the CO_2 savings achieved by the DSSTEG system over the course of a year. The maximum savings of 3.88 $kgyr^{-1}$ are obtained when the cooling heat transfer coefficient is 4 $kWm^{-2} K^{-1}$ and the absorbed solar flux is 40 kWm^{-2}. This indicates that the system, at its optimal operating conditions, can significantly contribute to reducing CO_2 emissions. On the other hand, the minimum savings of 0.45 $kgyr^{-1}$

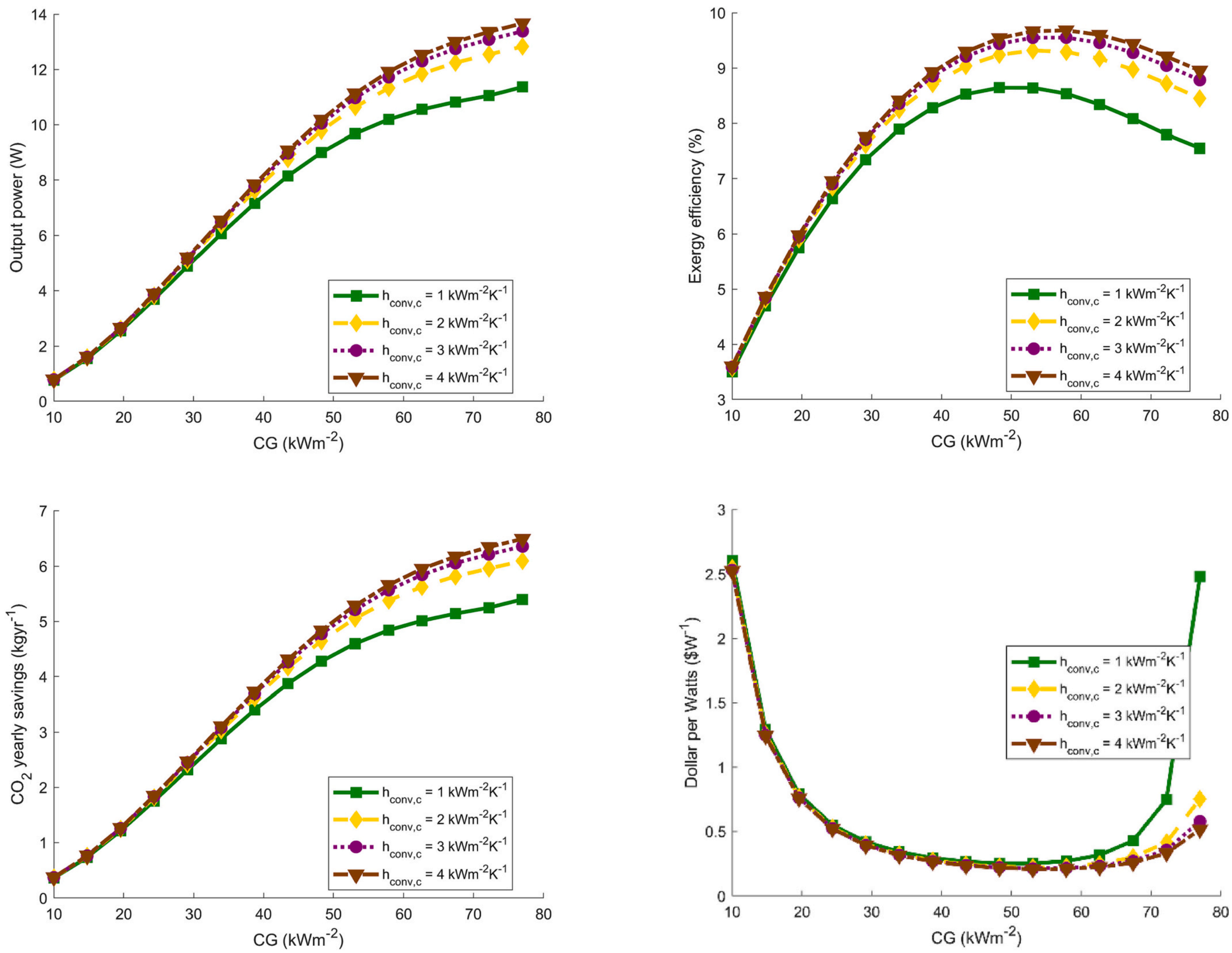

Fig. 4. Impacts of absorbed solar flux and cooling heat transfer coefficient on the DSSTEG's output power, exergy efficiency, yearly CO2 savings, and dollar per watts.

are achieved when the cooling heat transfer coefficient is 0.5 kWm^{-2} K^{-1} and the absorbed solar flux is 10 kWm^{-2}. This combination results in the lowest CO_2 reduction potential of the DSSTEG system. The dollars per watts metric provides insights into the economic feasibility of the DSSTEG system. The optimum value obtained is 0.25 $\$W^{-1}$, which occurs when the cooling heat transfer coefficient is 4 kWm^{-2} K^{-1} and the absorbed solar flux is 40 kWm^{-2}. This suggests that the system is cost-effective in terms of the amount of electrical power generated relative to the investment made. Conversely, the maximum value of 2.72 $\$W^{-1}$ is observed when the cooling heat transfer coefficient is 0.5 kWm^{-2} K^{-1} and the absorbed solar flux is 10 kWm^{-2}. This combination indicates higher costs per watt of power generated.

Our analysis provides an insightful look at the varying operational conditions of the Double-sided Skutterudite-based Solar Thermoelectric Generator (DSSTEG) system. Fig. 4 and Fig. 5 are particularly noteworthy as they offer a multifaceted perspective on the DSSTEG system's behavior and performance under different operational parameters.

In Fig. 4, we examine the influence of concentrated solar flux (ranging from 10 to 77 kW/m^2) and cooling Heat Transfer Coefficients (HTCs) ranging from 1 to 4 kW/m^2K. This representation provides an extensive understanding of how the DSSTEG system's performance responds to changing environmental and operational conditions. It illustrates the system's performance trends across a broad range of parameters, revealing the optimal solar flux and HTC values for maximizing output power under the defined geometric conditions.

On the other hand, Fig. 5 delves deeper into the performance of the DSSTEG system with an adjusted spectrum of concentrated solar flux levels specifically between 10 and 40 kW/m^2, while the HTC is varied. It offers a refined perspective, depicting the system's response to more narrow and specific operational conditions. This focused exploration provides an in-depth understanding of the parameter space where optimal power output is achieved.

While these figures may initially seem to present conflicting results, they are in fact offering complementary information. The results in Fig. 4 and Fig. 5 underscore the complex interplay between absorbed solar flux and the cooling HTC in determining the system's performance. They illuminate how different regions of the operational parameter space can lead to different optimal values for output power, exergy efficiency, CO_2 savings, and cost-effectiveness.

Moving forward, this detailed understanding of the DSSTEG system's performance across varied operational conditions is integral to our research. It informs our future goals of adopting a multi-objective optimization approach to simultaneously maximize power and efficiency, necessitating the careful negotiation of trade-offs between these key performance indicators. By doing so, we aim to enhance the effectiveness and efficiency of the DSSTEG system, contributing to the broader advancements in renewable energy systems.

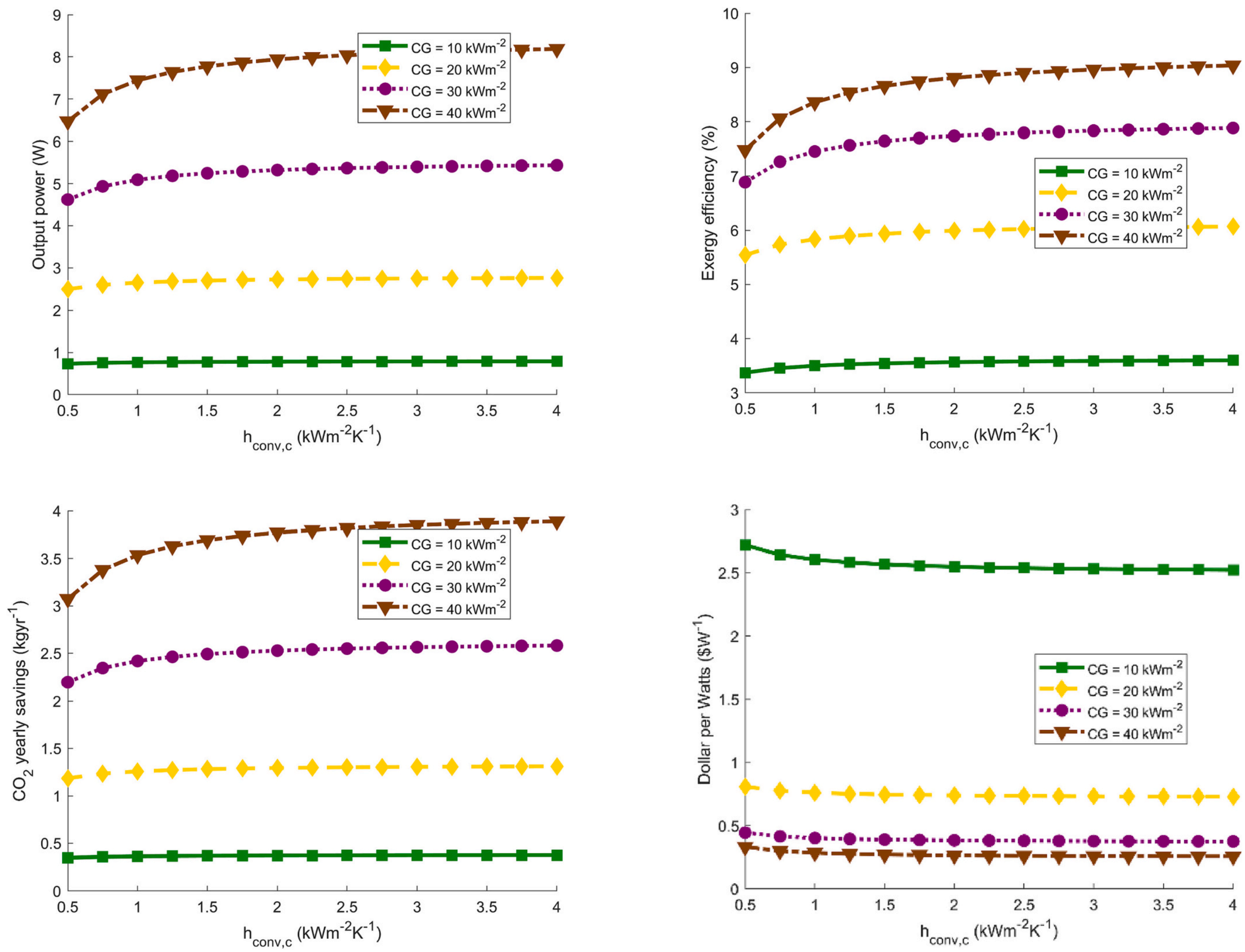

Fig. 5. Impacts of cooling heat transfer coefficient and absorbed solar flux on the DSSTEG's output power, exergy efficiency, yearly CO2 savings, and dollar per watts.

3.2. *Thermoelectric leg height*

The obtained results from Fig. 6 provides important insights into the system's output power. The maximum and optimal output power of 7.25 W, achieved at a thermoelectric leg height of 1.0 mm and an absorbed solar flux of 40 kWm^{-2}, indicates the highest level of power generation. This finding suggests that optimizing the system's design by adjusting the thermoelectric leg height and absorbed solar flux can significantly enhance its power output. On the other hand, the lower output power observed at a thermoelectric leg height of 14.0 mm highlights the importance of selecting appropriate design parameters to maximize power generation efficiency. The exergy efficiency of the DSSTEG system plays a crucial role in determining its overall performance. The highest exergy efficiency of 9.83% achieved at a thermoelectric leg height of 14.0 mm and an absorbed solar flux of 20 kWm^{-2} indicates the system's ability to convert concentrated solar energy into useful work with minimal losses. This finding emphasizes the importance of optimizing the system's design parameters to maximize exergy efficiency. Conversely, the lowest exergy efficiency observed at a thermoelectric leg height of 1.0 mm and an absorbed solar flux of 10 kWm^{-2} highlights the need for careful consideration of design parameters to avoid significant energy losses and inefficiencies in the conversion process. The analysis of CO_2 savings per year provides valuable information about the system's environmental impact. The optimal CO_2 savings of 3.44 $kgyr_{-1}$ achieved at a thermoelectric leg height of 1.0 mm and an absorbed solar flux of 40 kWm_{-2} demonstrate the system's potential to contribute to significant reductions in CO_2 emissions. This finding suggests that the DSSTEG system, when operated under specific conditions, can effectively support sustainable energy practices and mitigate climate change. The variation in CO_2 savings across different thermoelectric leg heights highlights the importance of selecting appropriate design parameters to optimize the system's environmental performance. The dollars per watts metric provides insights into the economic feasibility and cost-effectiveness of the DSSTEG system. The highest value obtained at 176.94 $\$W^{-1}$, occurring at a thermoelectric leg height of 14.0 mm and an absorbed solar flux of 10 kWm^{-2}, indicates a higher cost per watt of power generated which is not ideal for the system. This finding suggests that careful consideration of design parameters is necessary to balance economic factors and maximize cost-effectiveness. The optimum value of 0.17 $\$W^{-1}$ achieved at a thermoelectric leg height of 1.0 mm, applicable to all absorbed solar flux, demonstrates the potential for achieving a more favorable economic balance between installation costs and power generation. This highlights the importance of considering both technical and economic factors in optimizing the system's design.

In Fig. 7, the analysis reveals that the DSSTEG system achieves an optimal output power of 0.99 W at a thermoelectric leg height of 3.78 mm and a cooling heat transfer coefficient of 4 kWm^{-2} K^{-1}. This finding

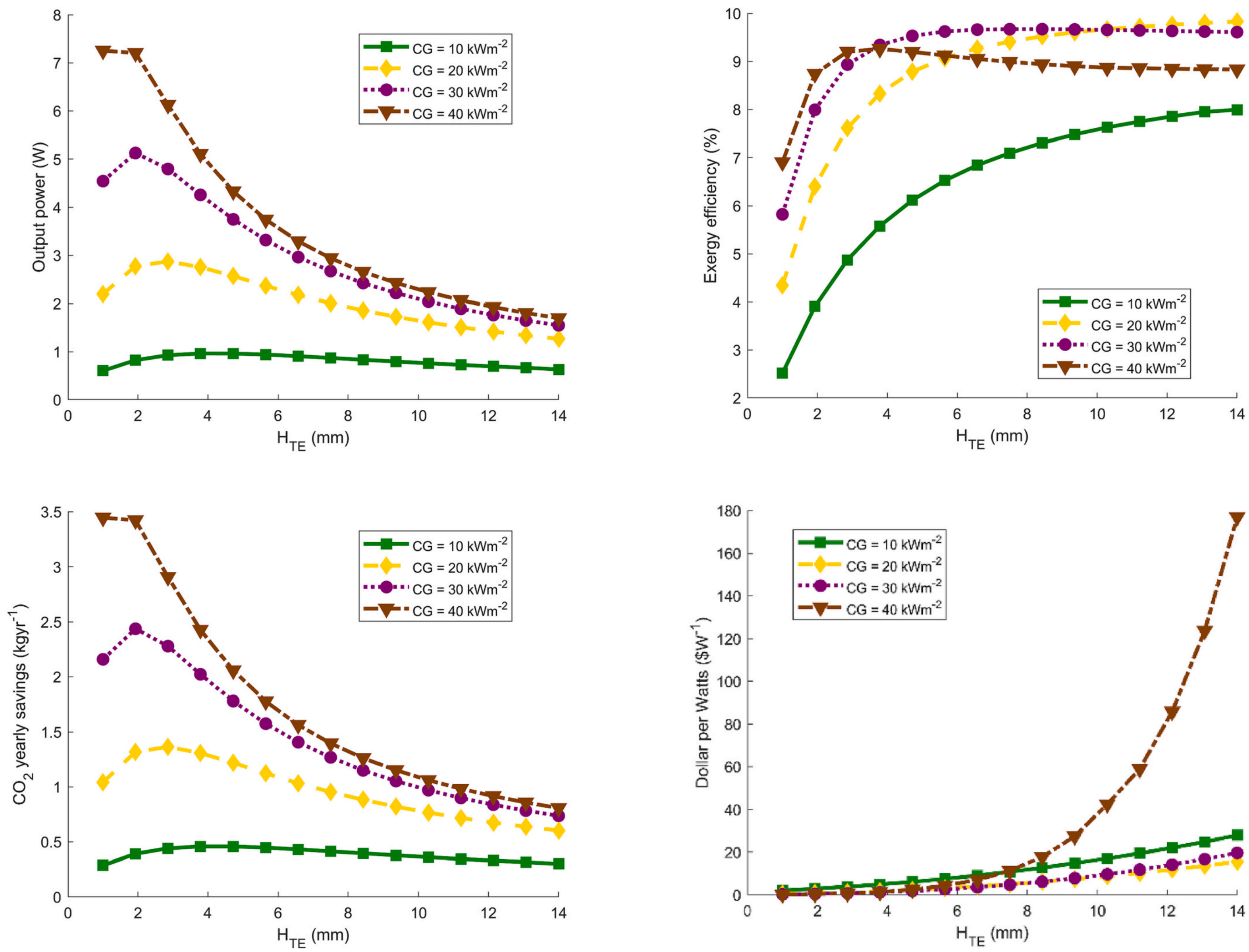

Fig. 6. Impacts of thermoelectric leg height and absorbed solar flux on the DSSTEG's output power, exergy efficiency, yearly CO2 savings, and dollar per watts.

indicates that there is an optimal combination of leg height and heat transfer coefficient that maximizes the system's power output. However, it is important to note that at greater thermoelectric leg heights, the output power declines significantly. This suggests that an improper selection of leg height can result in decreased power generation. Thus, careful consideration and optimization of the leg height parameter are crucial for achieving optimal output power in the DSSTEG system. Exergy efficiency measures the system's ability to convert energy into useful work effectively. The results demonstrate that the maximum exergy efficiency of 8.10% is achieved at a thermoelectric leg height of 14.0 mm, regardless of the cooling heat transfer coefficient. This indicates that a larger leg height is more favorable for improving exergy efficiency in the DSSTEG system. On the other hand, the lowest exergy efficiency of 2.51% is observed at a thermoelectric leg height of 1.0 mm, spanning across all cooling heat transfer coefficients. This finding highlights the importance of selecting an appropriate leg height to optimize the system's exergy efficiency. A suboptimal leg height can lead to reduced efficiency in converting solar energy into useful work. The analysis evaluates the CO_2 savings achieved by the DSSTEG system annually. The results indicate that the system saves its optimal CO_2 of 0.47 $kgyr^{-1}$ at a thermoelectric leg height of 3.78 mm and a cooling heat transfer coefficient of 4 kWm^{-2} K^{-1}. This implies that under these conditions, the system can significantly contribute to reducing CO_2 emissions. Conversely, the least CO_2 savings of 0.28 $kgyr^{-1}$ are observed at a thermoelectric leg height of 1.0 mm and a cooling heat transfer coefficient of 1 kWm^{-2} K^{-1}. This finding suggests that selecting an inappropriate leg height can lead to reduced CO_2 savings. Therefore, careful consideration of leg height is crucial for optimizing the system's environmental performance and minimizing carbon footprint. The dollars per watts metric provides insights into the economic feasibility of the DSSTEG system. The optimum value of 1.99 $$W^{-1}$ is achieved at a thermoelectric leg height of 1.0 mm for all cooling heat transfer coefficients. This suggests that, under these conditions, the system achieves a more favorable economic balance between installation costs and power generation. On the other hand, the dollars per watts value may not be optimal for other leg heights. This finding emphasizes the need to carefully consider the leg height parameter to ensure cost-effective operation of the DSSTEG system.

3.3. Thermoelectric leg cross-sectional area

In the investigation from Fig. 8, it was found that the DSSTEG system attains its highest power output of 7.64 W when the cross-sectional area of the thermoelectric leg is 2.56 mm^2 and the absorbed solar flux is 40 kWm^{-2}. This outcome suggests the existence of an optimal combination of leg area and solar flux that maximizes power generation in the system. Conversely, a substantial decrease in output power occurs when the absorbed solar flux is lower, specifically at 10 kWm^{-2}. Consequently, the solar flux plays a critical role in determining the system's power output. Hence, it is vital to carefully select the leg area and ensure an

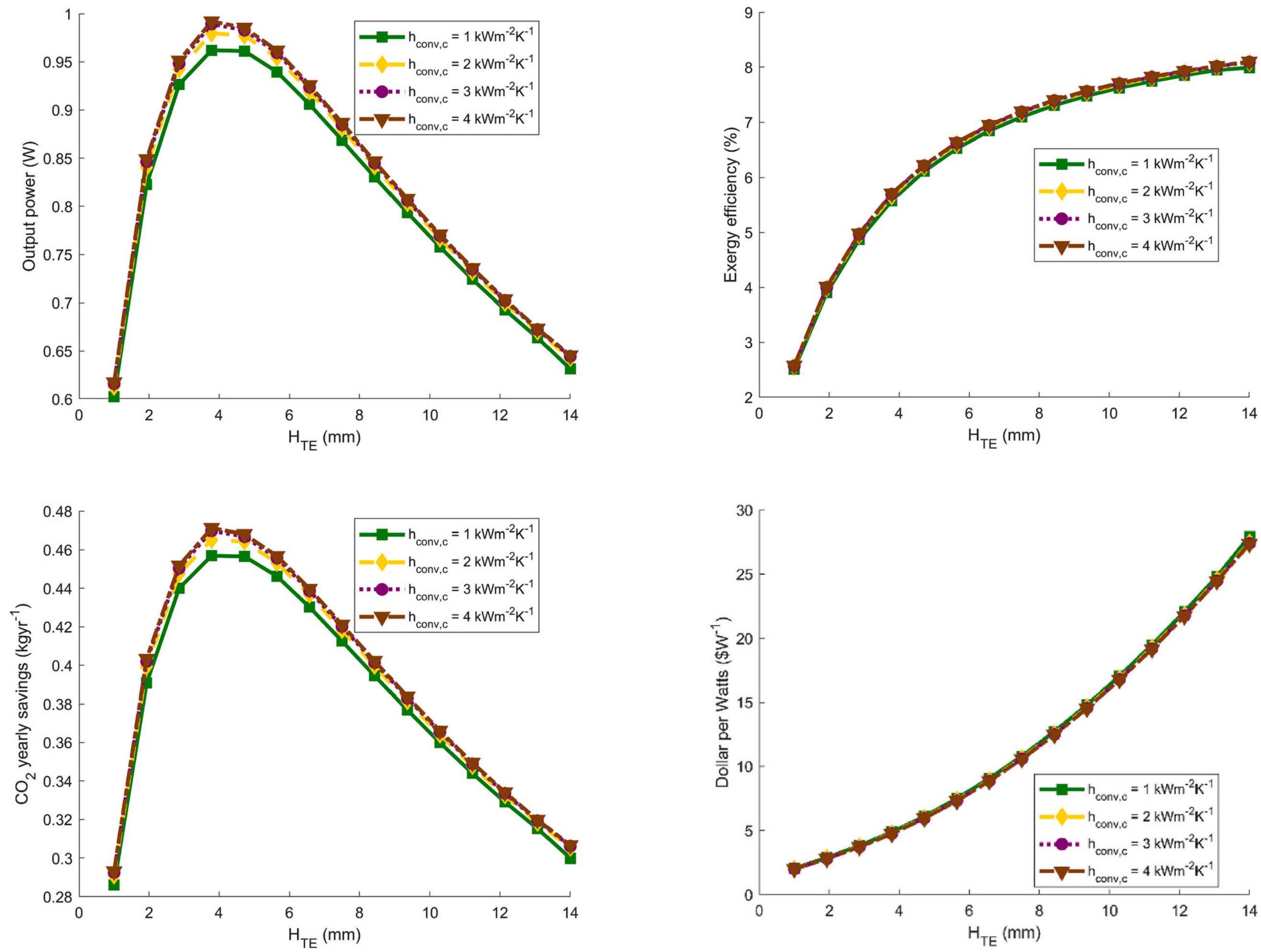

Fig. 7. Impacts of thermoelectric leg height and cooling heat transfer coefficient on the DSSTEG's output power, exergy efficiency, yearly CO2 savings, and dollar per watts.

appropriate absorbed solar flux to achieve maximum power generation. In regards to the exergy efficiency, which measures the system's effectiveness in converting energy into useful work, the research findings demonstrate that the highest efficiency of 8.94% is achieved when the cross-sectional area of the thermoelectric leg is 0.16 mm^2 and the absorbed solar flux is 30 kWm^{-2}. This indicates that a smaller leg area is more advantageous for improving exergy efficiency in the DSSTEG system. As the cross-sectional area increases, there is a steady decrease in the system's exergy efficiency. This emphasizes the significance of selecting an optimal leg area to maximize energy conversion efficiency. A larger leg cross-sectional area may lead to a less efficient conversion of solar energy into useful work. The investigation also evaluated the annual CO_2 savings achieved by the DSSTEG system. The results reveal that when the leg cross-sectional area of the thermoelectric leg is 2.56 mm^2 and the absorbed solar flux is 40 kWm^{-2}, the system saves a total of 3.63 $kgyr^{-1}$ of CO_2 per year. This highlights the system's potential for significant CO_2 reductions. However, it is important to note that the CO_2 savings may vary with changes in the leg cross-sectional area and absorbed solar flux. Therefore, optimizing the leg area and solar flux is crucial to maximize the environmental benefits of the DSSTEG system and reduce carbon emissions. Furthermore, the economic feasibility of the DSSTEG system was assessed using the dollars per watts metric. The optimal value of 0.22 $\$W^{-1}$ is achieved when the cross-sectional area of the thermoelectric leg is 0.64 mm^2 and the absorbed solar flux is 40 kWm^{-2}. This indicates that under these conditions, the system achieves a more favorable economic balance between installation costs and power generation. However, it should be noted that the dollars per watts value may vary for different cross-sectional areas and absorbed solar flux levels. This emphasizes the importance of carefully considering the leg area parameter to ensure cost-effective operation of the DSSTEG system.

The analysis in Fig. 9 revealed that an optimal output power of 1.39 W was achieved when the thermoelectric leg cross-sectional area was 0.09 mm^2, regardless of the cooling heat transfer coefficient. This indicates that there is an ideal leg area that maximizes the system's power generation potential. On the other hand, the lowest output power of 0.76 W was observed at a larger leg cross-sectional area of 2.56 mm^2, also across all cooling heat transfer coefficients. These findings highlight the importance of selecting an appropriate leg area to achieve higher power output in the DSSTEG system. Additionally, it suggests that the cooling heat transfer coefficient does not significantly impact the system's output power within the tested range of values. The highest exergy efficiency of 7.26% was attained at a thermoelectric leg cross-sectional area of 0.04 mm^2, regardless of the cooling heat transfer coefficient. This implies that a smaller leg area contributes to improved energy conversion efficiency in the system. Conversely, the lowest exergy efficiency of 3.30% was observed at a larger leg cross-sectional area of 2.56 mm^2, specifically with a cooling heat transfer coefficient of 1 $kWm^{-2}\ K^{-1}$. These results indicate that selecting a smaller leg area is crucial for enhancing the system's exergy efficiency. Furthermore, it suggests that the choice of cooling heat transfer coefficient can influence the system's energy conversion efficiency. CO_2 Savings per Year: The analysis

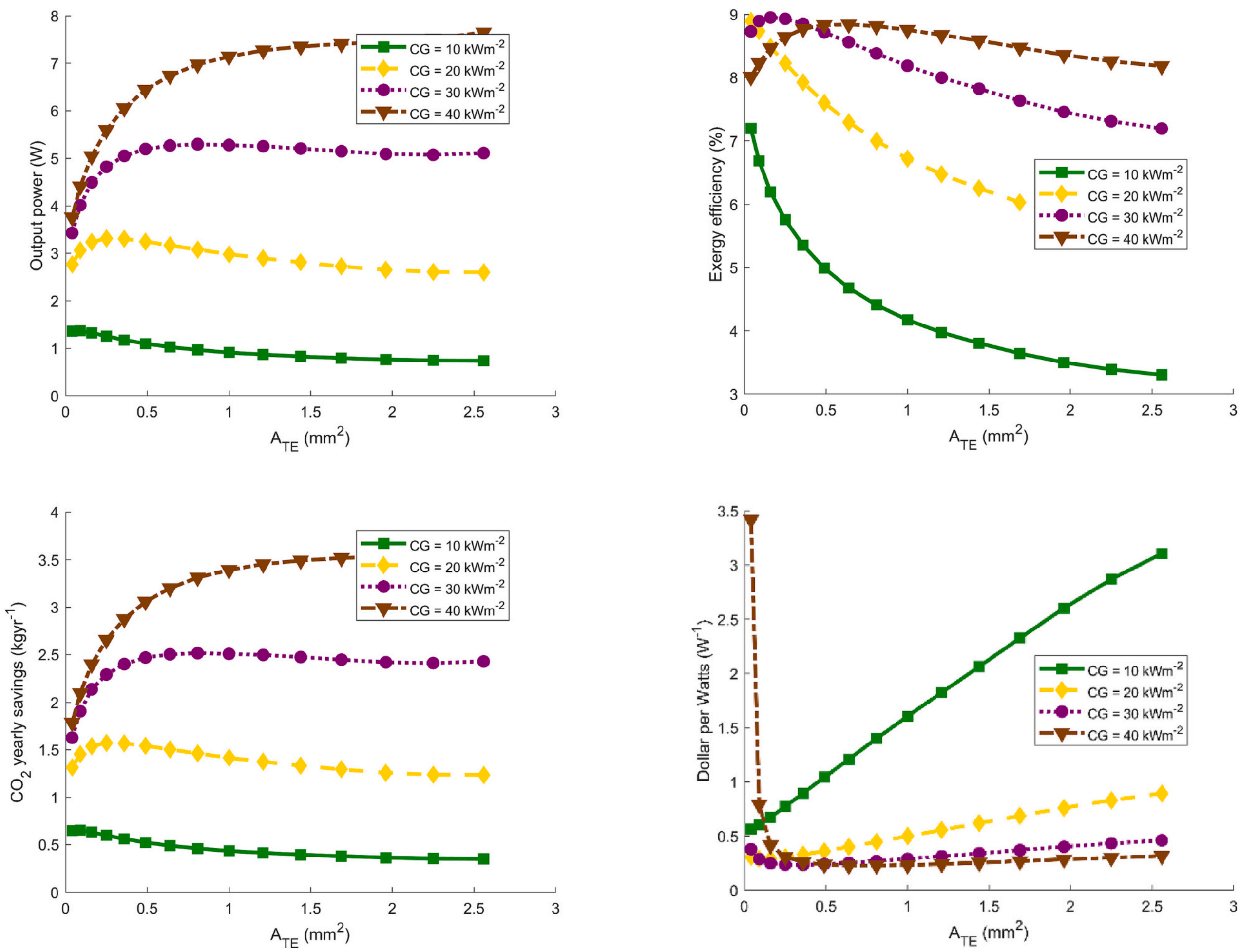

Fig. 8. Impacts of thermoelectric leg cross-sectional area and absorbed solar flux on the DSSTEG's output power, exergy efficiency, yearly CO2 savings, and dollar per watts.

demonstrated that the system achieved the highest yearly CO_2 savings of 0.66 $kgyr^{-1}$ when the thermoelectric leg cross-sectional area was 0.09 mm^2, coupled with a cooling heat transfer coefficient of 4 kWm^{-2} K^{-1}. Conversely, the lowest CO_2 savings per year of 0.36 $kgyr^{-1}$ were observed at a larger leg cross-sectional area of 2.56 mm^2, with a cooling heat transfer coefficient of 1 kWm^{-2} K^{-1}. These findings emphasize the significance of selecting an optimal leg area and cooling heat transfer coefficient to maximize the system's environmental benefits. It suggests that a smaller leg area and a higher cooling heat transfer coefficient contribute to greater CO_2 reduction potential. The dollars per watts metric provides insights into the economic feasibility of the DSSTEG system. The optimal value of 0.55 $\$W^{-1}$ was achieved at a thermoelectric leg cross-sectional area of 0.04 mm^2, specifically with a cooling heat transfer coefficient of 1 kWm^{-2} K^{-1}. This indicates that, under these conditions, the system achieves a more cost-effective balance between installation costs and power generation. Conversely, the worst-case scenario of 3.10 $\$W^{-1}$ was observed at a larger leg cross-sectional area of 2.56 mm^2, across all cooling heat transfer coefficients. These findings underscore the importance of selecting an optimal leg area and cooling heat transfer coefficient to ensure the economic viability of [the] DSSTEG system.

3.4. Percentage content of skutterudite

Output power from Fig. 10 is a crucial parameter in assessing the effectiveness of the DSSTEG system in converting solar energy into electricity. The analysis revealed that the system achieved its maximum output power of 50.08 W at a skutterudite content of 6.17% and an absorbed solar flux of 40 kWm^{-2}. This finding indicates that an optimal combination of skutterudite content and solar flux can significantly enhance power generation. Conversely, the system experienced the lowest output power of 0.36 W at a higher skutterudite content of 92.56% and a lower absorbed solar flux of 10 kWm^{-2}. This result highlights the importance of finding an appropriate balance between skutterudite content and solar flux to maximize power output. For exergy efficiency, the study demonstrated that the highest exergy efficiency of 16.93% was achieved at a skutterudite content of 6.17% and an absorbed solar flux of 30 kWm^{-2}. This suggests that an optimal amount of skutterudite content can enhance the system's energy conversion efficiency. On the other hand, the lowest exergy efficiency of 1.88% was observed at a higher skutterudite content of 92.56% and a lower absorbed solar flux of 10 kWm^{-2}. This result emphasizes the need to carefully consider the skutterudite content to achieve higher exergy efficiency in the DSSTEG system. CO_2 savings per year is an important metric for assessing the environmental impact of the DSSTEG system. The analysis revealed that the system achieved its highest CO_2 savings of 23.78 $kgyr^{-1}$ at a skutterudite content of 6.17% and an absorbed solar flux of 40 kWm^{-2}. This finding highlights the potential of the DSSTEG system to contribute significantly to reducing carbon emissions. Conversely, the lowest CO_2 savings of 0.17 $kgyr^{-1}$ were observed at a higher skutterudite content of 92.59% and a lower absorbed solar flux of 10 kWm^{-2}. This result emphasizes the importance of optimizing the skutterudite content to maximize CO_2 savings and enhance the system's environmental benefits. The economic feasibility of the DSSTEG system

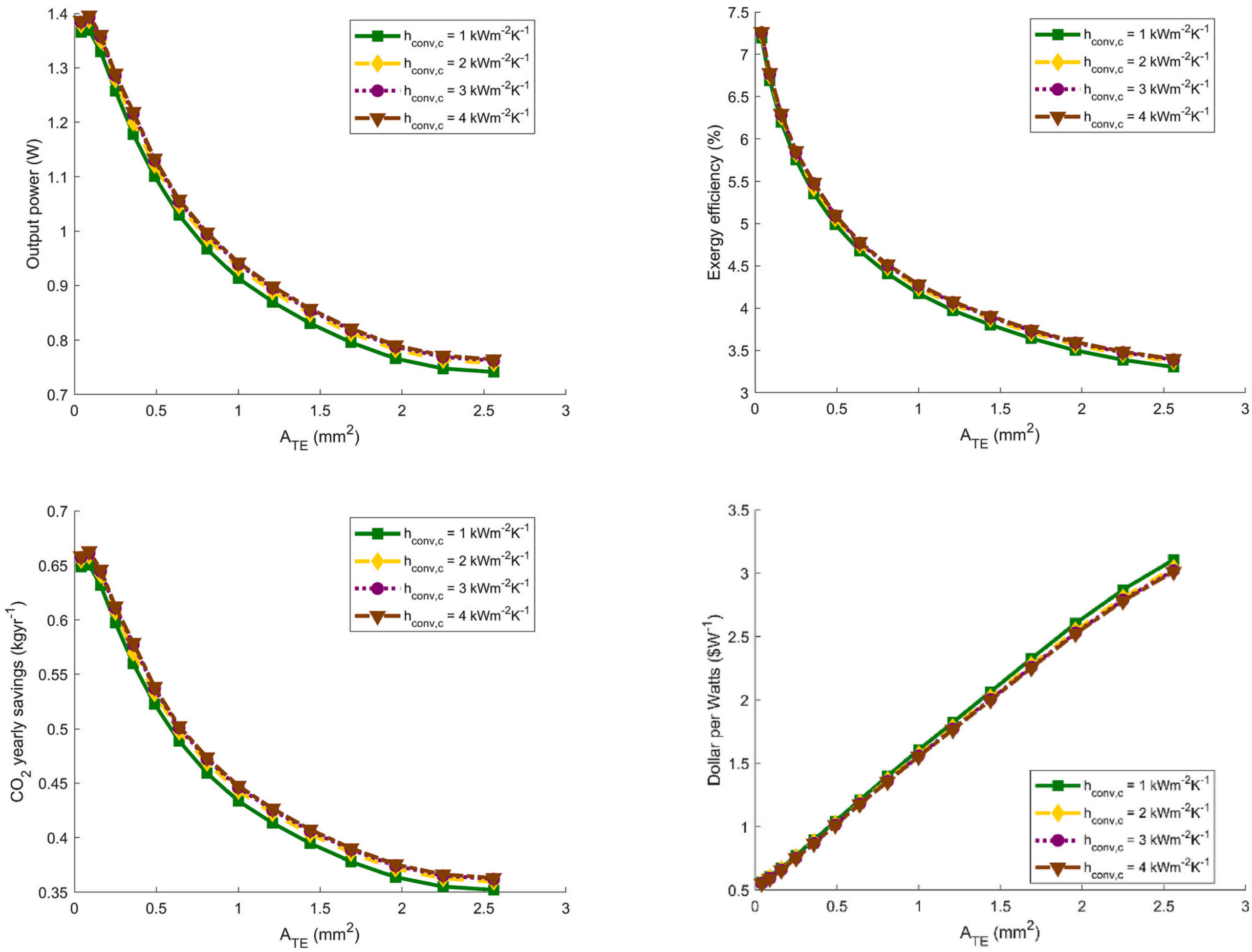

Fig. 9. Impacts of thermoelectric leg cross-sectional area and cooling heat transfer coefficient on the DSSTEG's output power, exergy efficiency, yearly CO2 savings, and dollar per watts.

can be evaluated using the dollars per watts metric. The study found that the optimal dollars per watts ratio of 0.05 $\$W^{-1}$ was achieved at a skutterudite content of 6.17% and an absorbed solar flux of 10 kWm^{-2}. This indicates that under these conditions, the system achieved a more favorable economic balance between installation costs and power generation. It is important to note that the dollars per watts ratio may vary for different skutterudite contents and absorbed solar flux levels, underscoring the need for careful consideration of these parameters to ensure cost-effectiveness.

From Fig. 11, output power is a crucial factor when assessing the efficacy of the DSSTEG system in converting concentrated solar energy into electrical power. The analysis indicated that the system attained its peak output power of 8.81 W when the skutterudite content was 6.17%, regardless of the cooling heat transfer coefficients. This suggests that an optimal skutterudite content significantly enhances power generation. Conversely, the system exhibited the lowest output power of 0.37 W when the skutterudite content was 92.59%, across all cooling heat transfer coefficients. This underscores the importance of striking the right balance in skutterudite content to maximize power output. Exergy efficiency gauges the system's ability to effectively convert available energy into useful work. The study found that the maximum exergy efficiency of 10.18% was achieved at a skutterudite content of 6.17% across all cooling heat transfer coefficients. This indicates that an optimal skutterudite content enhances the system's energy conversion efficiency. Conversely, the lowest exergy efficiency of 1.88% was observed when the skutterudite content was 92.59%, regardless of the cooling heat transfer coefficients. This result highlights the need for careful consideration of skutterudite content to achieve higher exergy efficiency in the DSSTEG system. CO_2 savings per year serves as a vital metric for evaluating the environmental impact of the DSSTEG system. The analysis demonstrated that the highest CO_2 savings per year, amounting to 4.18 $kgyr^{-1}$, were achieved at a skutterudite content of 6.17% across all cooling heat transfer coefficients. This finding underscores the potential of the DSSTEG system to significantly contribute to reducing carbon emissions. Conversely, the lowest CO_2 savings per year of 0.17 $kgyr^{-1}$ were observed when the skutterudite content was 92.59%, regardless of the cooling heat transfer coefficients. This result highlights the significance of optimizing the skutterudite content to maximize CO_2 savings and enhance the system's environmental benefits. To summarize, the results indicate that both the amount of skutterudite content and cooling heat transfer coefficient exert significant influences on the DSSTEG system's output power, exergy efficiency, and CO_2 savings per year. An optimal skutterudite content of 6.17% leads to higher output power, exergy efficiency, and CO_2 savings, while a higher skutterudite content of 92.59% diminishes performance in these parameters. These findings emphasize the criticality of meticulous selection and optimization of skutterudite content and cooling heat transfer coefficient to maximize the overall performance and environmental sustainability of the DSSTEG system. Further analysis and optimization in these areas can contribute to the advancement of more efficient and environmentally friendly technologies for concentrated solar energy conversion.

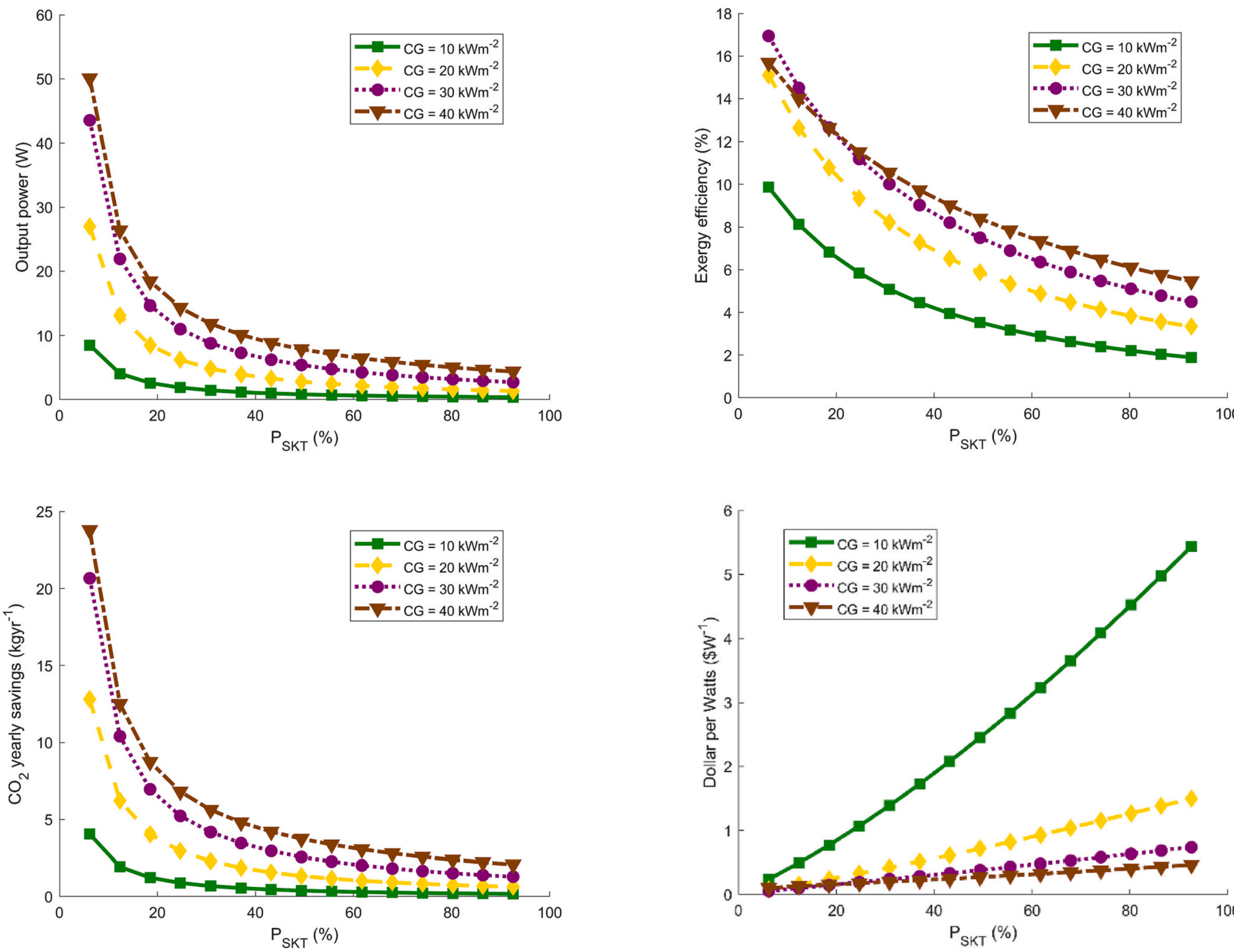

Fig. 10. Impacts of amount of skutterudite content and absorbed solar flux on the DSSTEG's output power, exergy efficiency, yearly CO2 savings, and dollar per watts.

3.5. Design parameters and heat dynamics in TEGs

In our investigation, we thoroughly assessed the impact of modifying key parameters - thermoelectric (TE) leg height, cross-sectional area, and skutterudite content, under varying heating and cooling conditions. The trends we observed in our results stem from the intricate interplay between these parameters and the mechanisms of heat absorption and rejection at the hot and cold junctions of the TE generator.

For instance, let's consider the modification of the TE leg's height. Such a change inherently alters the thermal conductance of these legs. The resultant shift in conductance dictates a greater absorption of heat flux at the hot junction, which consequentially elevates the thermal gradient across the TE generator.

This rise in thermal gradient ushers in fluctuating operating temperatures within the TE semiconductors. These temperature fluctuations, in turn, dynamically influence the performance of material properties critical to the TE generator's operation. Key among these properties are the Seebeck coefficient, electrical resistivity, and thermal conductivity - each exhibiting their own optimal performance conditions that shift with the changing thermal environment.

This detailed examination of parameter influence and resultant trends offers valuable insights into the performance optimization of thermoelectric generators. By understanding the effects of these crucial design elements and their interactions, we can more accurately guide the development of efficient, tailored TE generators for concentrated solar energy conversion.

3.6. 4E optimization insights

The obtained optimization values in the analysis provides crucial insights into the performance and potential of the DSSTEG system.

1. **Optimal Output Power**: The system achieved an impressive output power of 50.08 W at the optimal skutterudite content of 6.17%. This signifies that the chosen composition of skutterudite material maximizes the system's capability to convert concentrated solar energy into usable electrical power. The higher output power is of great significance as it directly impacts the system's energy generation capacity and its ability to meet power demands.
2. **Optimal Exergy Efficiency:** Exergy efficiency is a measure of how effectively a system converts available energy into useful work. The obtained optimal exergy efficiency of 16.93% at 6.17% skutterudite content indicates that this composition allows for efficient energy conversion within the DSSTEG system. It implies that the system can extract a larger portion of the available energy and convert it into usable electrical power, minimizing energy losses in the process.
3. **Optimum Yearly CO_2 Savings:** The optimal yearly CO_2 savings of 23.78 $kgyr^{-1}$ achieved at the skutterudite content of 6.17% highlights the environmental benefits of the DSSTEG system. By utilizing concentrated solar energy and reducing reliance on fossil fuel-based

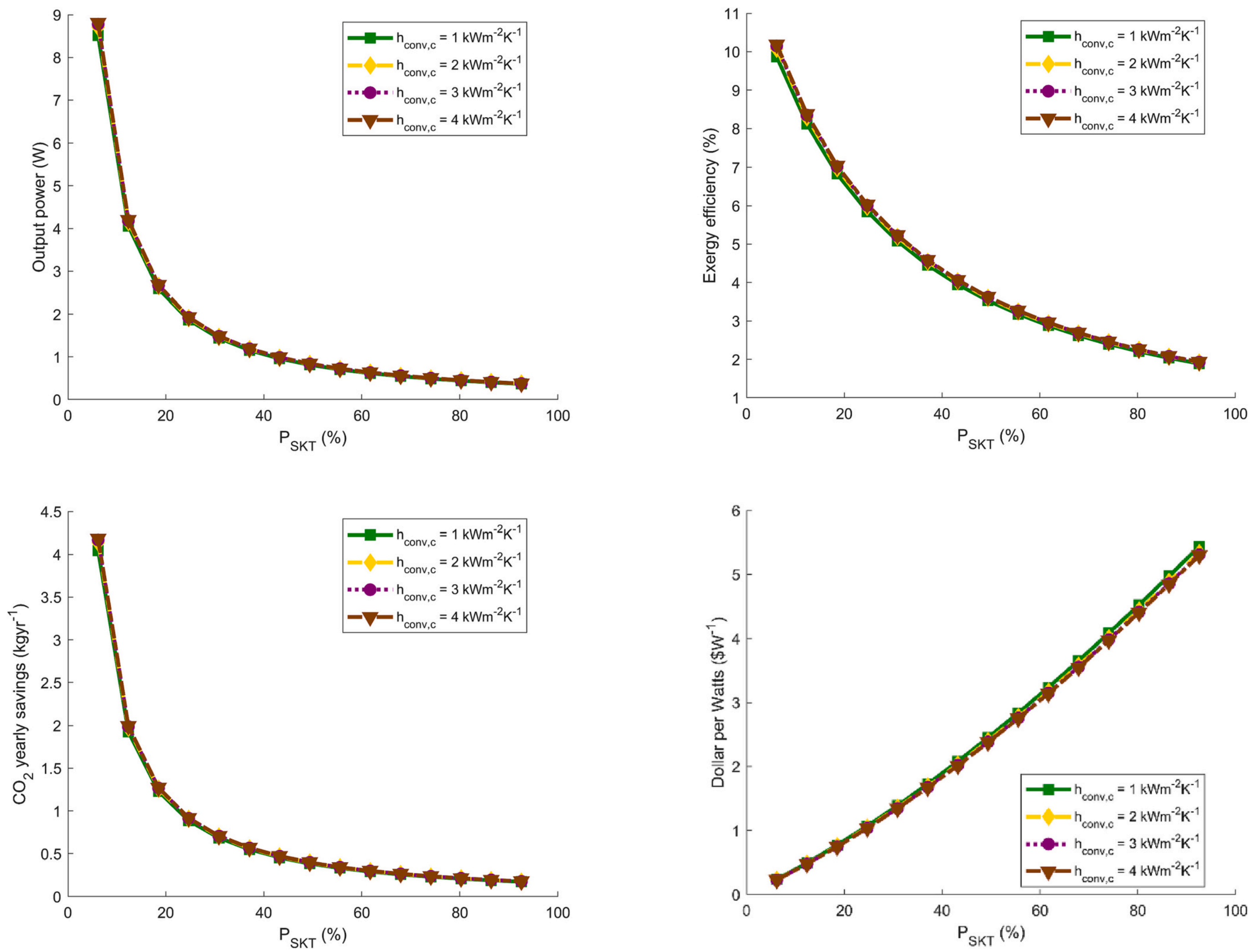

Fig. 11. Impacts of thermoelectric leg cross-sectional area and cooling heat transfer coefficient on the DSSTEG's output power, exergy efficiency, yearly CO2 savings, and dollar per watts.

power generation, the system contributes significantly to lowering carbon emissions. This finding is of utmost importance in addressing climate change and promoting sustainable energy solutions.

4. **Optimal Dollars per Watts Ratio:** The obtained optimal dollars per watts ratio of 0.05 $\$W^{-1}$ at 6.17% skutterudite content indicates the cost-effectiveness of the DSSTEG system. This ratio represents the financial efficiency of the system, reflecting the balance between installation costs and the generated power output. The low value suggests that the system offers a favorable return on investment, making it an economically viable option for concentrated solar energy conversion.

These optimal values collectively demonstrate the potential and advantages of the DSSTEG system with a skutterudite content of 6.17%. It showcases the system's ability to generate higher power output, achieve efficient energy conversion, contribute to significant CO_2 savings, and provide a cost-effective solution for concentrated solar energy conversion. The findings emphasize the importance of selecting the optimal skutterudite content to maximize the system's performance and overall efficiency.

3.7. Optimized modules

The optimized parameters utilized in the design of the DSSTEG to achieve maximum 4E performance, and a comparison with unoptimized modules operating under identical thermal and geometric parameters, are shown in Table 2. This comparison provides an overview of the effectiveness of the optimization strategy deployed in this study.

For visualization, three-dimensional nephograms of temperature and electrical voltage constructed from the optimal design parameters are depicted in Fig. 12 (for maximum power, P_{max}, and CO_2 yearly savings,

Table 2
Optimal parameters for 4E performance and comparisons with unoptimized module.

Parameter	P_{max} & $CO_{2,max}$		$\eta_{ex,max}$ & DPW_{min}	
	Optimal module	Unoptimized module	Optimal module	Unoptimized module
CG	40 kWm^{-2}	40 kWm^{-2}	30 kWm^{-2}	30 kWm^{-2}
h_{convc}	1 kWm^{-2} K^{-1}	1 kWm^{-2} K^{-1}	1 kWm^{-2} K^{-1}	1 kWm^{-2} K^{-1}
H_{TE}	1.62 mm	1.62 mm	1.62 mm	1.62 mm
A_{TE}	1.96 mm^2	1.96 mm^2	1.96 mm^2	1.96 mm^2
P_{SKT}	*6.17%*	*50%*	*6.17%*	*50%*
P_{max}	**50.1 W**	7.7 W	43.5 W	5.3 W
$CO_{2,max}$	**23.8 $kgyr^{-1}$**	3.7 $kgyr^{-1}$	20.7 $kgyr^{-1}$	2.5 $kgyr^{-1}$
$\eta_{ex,max}$	15.7%	8.5%	**16.9%**	7.6%
DPW_{min}	0.1 $\$W^{-1}$	0.3 $\$W^{-1}$	**0.05 $\$W^{-1}$**	0.4 $\$W^{-1}$

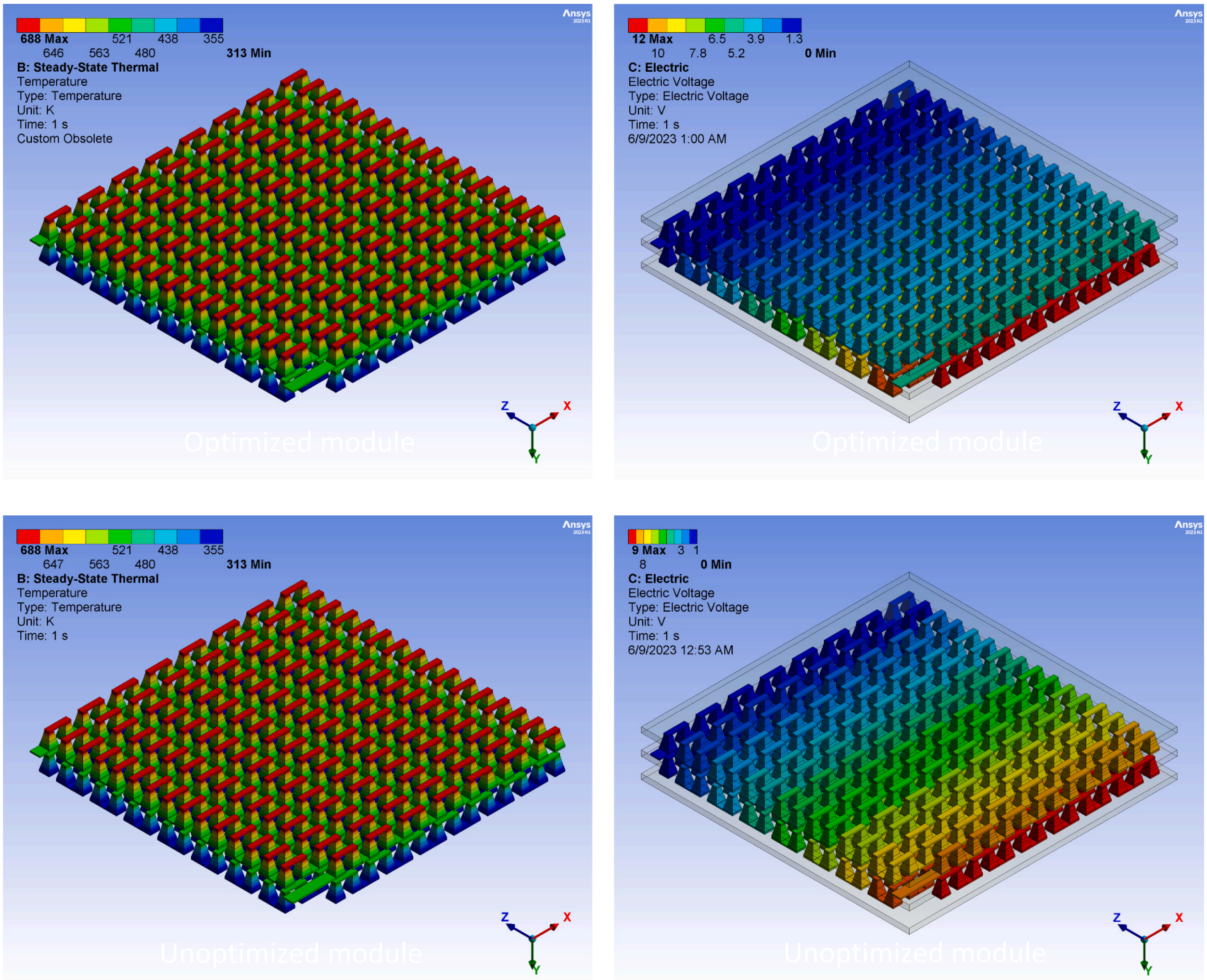

Fig. 12. Three-dimensional temperature and voltage distributions for a module optimized for maximum power and CO_2 savings.

$CO_{2,max}$) and Fig. 13 (for maximum exergy efficiency, $\eta_{ex,max}$, and minimum dollar per watt, DPW_{min}).

An examination of the nephograms reveals that while the hot and cold junction temperatures of the optimized and unoptimized modules appear similar, the latter generates a larger electrical voltage. This can be attributed to temperature variations within the interfaces of the different semiconductors that make up the optimized module. These variations lead to higher intermediate temperature ranges which subsequently generate a larger electrical voltage by leveraging the Seebeck effect.

According to Table 2, the optimized module achieves power and CO_2 savings of 50.1 W and 23.8 $kgyr^{-1}$, respectively. Conversely, the unoptimized module, when operated under identical thermal conditions, provides a power output and CO_2 savings of 7.7 W and 3.7 $kgyr^{-1}$, respectively. This comparison indicates that the optimization strategy improved the power and CO_2 savings of the unoptimized system by a factor of 6.5.

Simultaneously, the optimized module yields a maximum exergy efficiency of 16.9% at a minimum cost of 0.05 $/W. In contrast, the unoptimized module achieves an efficiency of 7.6% and a cost of 0.4 $/W under the same conditions. This demonstrates that the optimization strategy more than doubled the efficiency of the unoptimized module while reducing the operating cost by 86%.

Considering the system from a different perspective, operating under maximum power and CO_2 conditions resulted in an exergy efficiency and cost of 15.7% and 0.1 $/W, respectively. This corresponds to a reduction in peak exergy efficiency by 7.4%, while the optimal operating cost increased by 94%. Alternatively, operating the system under conditions for maximum efficiency yielded 43.5 W of power and 20.7 $kgyr^{-1}$ in CO_2 savings, indicating a 15.1% reduction in both power generation capacity and annual CO_2 savings.

4. Conclusions

In this trailblazing study, we have pioneered a comprehensive analysis of double-stage segmented thermoelectric generators (DSSTEGs) optimized for concentrated solar energy conversion. Leveraging the power of finite element analysis in ANSYS, we thoroughly explored the relationship between geometric parameters, skutterudite content, and solar energy concentration, aiming to unlock the full potential of DSSTEG technology.

Our research has resulted in several groundbreaking discoveries and improvements in DSSTEG design and performance:

i. *Optimal Thermoelectric Leg Geometry*: Through meticulous geometric fine-tuning, we identified an optimal thermoelectric leg height of 1.0 mm, which led to peak power output (7.25 W) and remarkable exergy efficiency (8.94%). This achievement demonstrates the critical role of geometric parameters in enhancing the performance of DSSTEGs.

ii. *Skutterudite Content Advancement:* Our economic analysis revealed that incorporating skutterudite at a concentration of

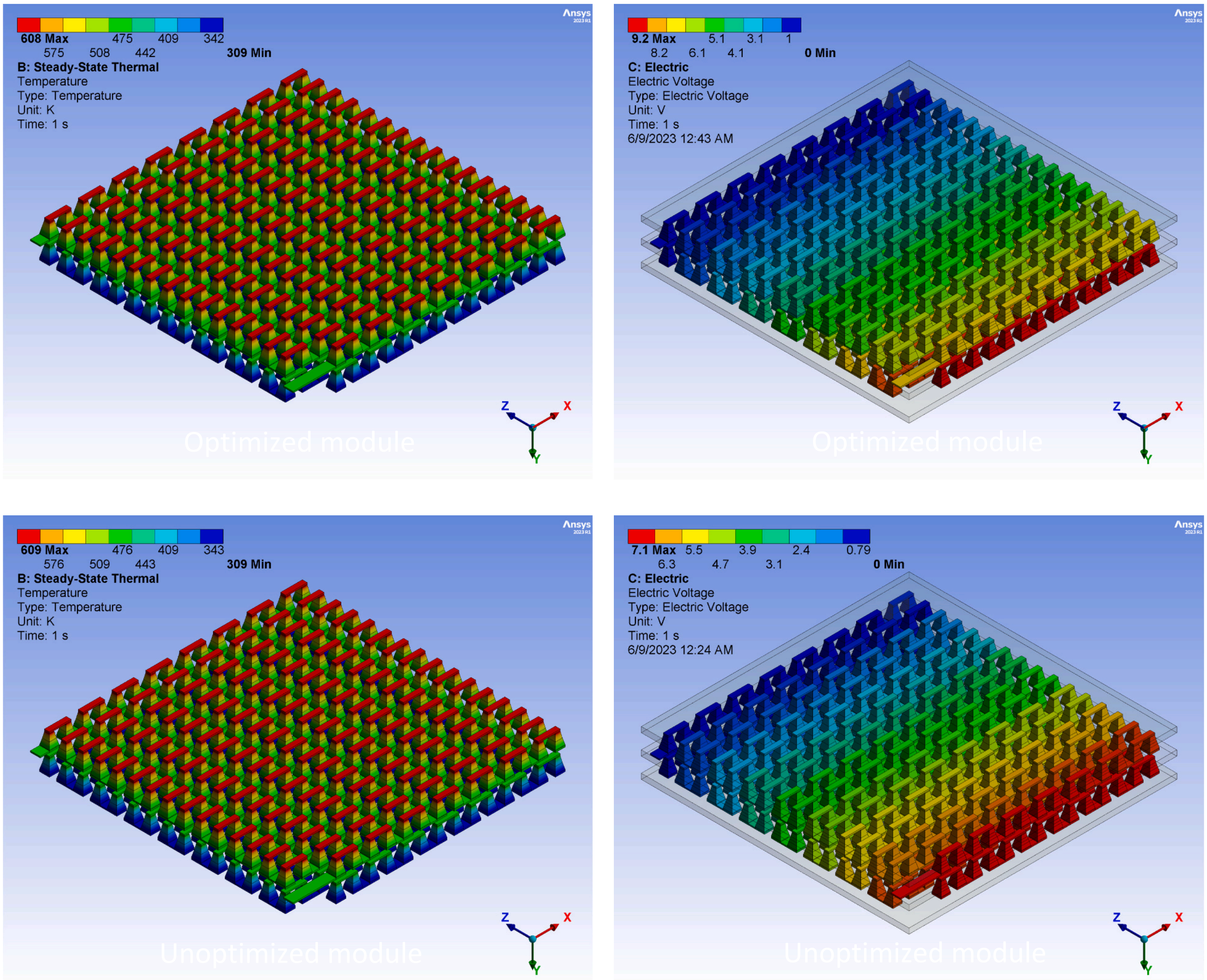

Fig. 13. Three-dimensional temperature and voltage distributions for a module optimized for maximum exergy efficiency and minimum DPW.

6.17% significantly boosts DSSTEG performance. This advancement resulted in an impressive power generation capacity of 50.1 W, a CO_2 emissions reduction of 23.8 kg/year, and an unmatched exergy efficiency of 16.9% at an operating cost as low as 0.05 $\$W^{-1}$. These findings underscore the pivotal role of material composition in optimizing DSSTEG performance.

iii. *Power-Efficiency Trade-off Optimization:* Our study unveiled a trade-off between maximum power conditions and exergy efficiency. However, through strategic parameter configurations, we demonstrated the potential to optimize both power output and efficiency without significant compromise. This insight opens up new possibilities for achieving a balance between power generation and energy conversion efficiency in DSSTEGs.

The implications of these discoveries are profound, as they provide a revolutionary compass for scientists, engineers, and industry experts in DSSTEG design. The optimized DSSTEG configurations presented in this study stand as a major improvement in sustainable energy solutions. By leveraging the insights gleaned from this research, we have laid the foundation for the design of next-generation thermoelectric generators, optimized for energy, exergy, environmental impact, and economics.

In conclusion, this study represents a significant improvement in the field of thermoelectric generators, particularly in the realm of concentrated solar energy conversion. The advancements made in DSSTEG technology position it as a key player in the pursuit of sustainable and cleaner energy solutions. By combining innovative design approaches, strategic material selection, and meticulous optimization, we move closer to a future powered by efficient, eco-friendly, and economically viable thermoelectric generators.

5. Limitations of the study

The limitations of our study are as follows:

i. *Simplified Modeling Assumptions*: Our study utilized numerical simulations based on finite element analysis in ANSYS, which involved certain simplifications in the model. Real-world scenarios may introduce complexities that were not fully considered in our simulations.
ii. *Absence of Experimental Validation:* The lack of experimental validation is a limitation of our study. While numerical simulations are useful for understanding the behavior of DSSTEGs under specific conditions, real-world experimental validation is essential to verify the accuracy of the simulation results and validate the performance of DSSTEGs under practical operating conditions.

By recognizing these limitations, we aim to underscore the importance of future research to address these gaps and improve the overall understanding and practical application of DSSTEG technology. The future studies section serves as a roadmap for researchers to further advance the field and overcome the identified limitations.

6. Future studies

Further research on the performance analysis and optimization of Double Stage Segmented Thermoelectric Generators (DSSTEGs) for concentrated solar energy conversion can explore several novel aspects to advance the field and address potential limitations.

- **Advanced Materials Investigation:** Investigations can look into the use of novel thermoelectric materials with improved properties, such as higher Seebeck coefficient, lower thermal conductivity, and enhanced stability at high temperatures. Explore emerging materials, such as hybrid organic-inorganic perovskites or nanostructured materials, to enhance the overall performance and efficiency of DSSTEG systems.
- **Integrated Heat Recovery Systems:** Future studies can advance towards the integration of heat recovery systems in DSSTEGs to enhance overall system efficiency. Explore the utilization of waste heat from the system for additional power generation or other applications. This can involve the incorporation of secondary heat transfer loops or the integration of heat exchangers to recover and utilize waste heat effectively.
- **Optimal Control and Power Management:** Researchers can develop advanced control and power management strategies for DSSTEG systems. Investigate intelligent algorithms and optimization techniques to dynamically adjust parameters such as absorbed solar flux, cooling heat transfer coefficient, and load resistance to maximize overall system performance. Consider the integration of machine learning and artificial intelligence algorithms for adaptive control and optimization.
- **Reliability and Durability Studies:** Comprehensive studies on the reliability and durability of DSSTEG systems can be conducted. Investigate the long-term performance and degradation mechanisms of thermoelectric modules under concentrated solar radiation and high-temperature conditions. Evaluate the effects of thermal cycling, environmental factors, and aging on the performance and stability of the system. Develop mitigation strategies to improve the durability of DSSTEG systems.
- **Comprehensive Life Cycle Assessment (LCA)**: Future studies should focus on the detailed LCA of DSSTEGs, a crucial aspect that extends beyond the operational efficiency of these systems. These assessments would evaluate the environmental impact of DSSTEGs from the raw material extraction stage through manufacturing, operation, transportation, and finally, to end-of-life disposal. Such a holistic approach will offer a clearer understanding of the overall environmental footprint of DSSTEGs, enabling a comparison of the optimized DSSTEG system with other configurations and technologies in terms of their complete life cycle impacts.

CRediT authorship contribution statement

Hisham Alghamdi: Investigation, Resources, Writing – original draft, Writing – review & editing. **Chika Maduabuchi:** Writing – original draft, Validation, Supervision, Software, Resources, Project administration, Methodology, Investigation, Formal analysis, Conceptualization. **Kingsley Okoli:** Writing – original draft, Visualization, Investigation, Formal analysis. **Abdullah Albaker:** Data curation, Formal analysis, Methodology, Validation. **Emad Makki:** Data curation, Funding acquisition, Investigation, Resources. **Mohammed Alghassab:** Investigation, Methodology, Project administration, Visualization, Writing – review & editing. **Mohammad Alobaid:** Formal analysis, Project administration, Supervision, Visualization. **Mohammad Alkhedher:** Formal analysis, Investigation, Supervision, Validation, Visualization, Writing – review & editing.

Declaration of Competing Interest

The authors declare that they have no known competing financial interests or personal relationships that could have appeared to influence the work reported in this paper.

Data availability

The data that has been used is confidential and cannot be disclosed at the moment.

Acknowledgments

The authors are thankful to the following funding sources: The Deanship of Scientific Research at Najran University for funding this work under the Research Priorities and Najran Research funding program grant code (NU/NRP/SERC/12/16), the Deanship of Scientific Research, Majmaah University, Saudi Arabia for funding this research work through the project number (ICR-2023-599), the Deanship of Scientific Research at Shaqra University for supporting this work, the Office of Research and Sponsored Programs (ORSP) at Abu Dhabi University for funding this paper through a research fund.

References

[1] Seebeck TJ. Ueber die magnetische Polarisation der Metalle und Erze durch Temperaturdifferenz. Ann Phys 1826;82:253–86. https://doi.org/10.1002/andp.18260820302.
[2] Ali H, Yilbas BS, Al-Sulaiman FA. Segmented thermoelectric generator: influence of pin shape configuration on the device performance. Energy 2016;111:439–52. https://doi.org/10.1016/j.energy.2016.06.003.
[3] Badillo-Ruiz C, Olivares-Robles M, Ruiz-Ortega P. Performance of segmented thermoelectric cooler micro-elements with different geometric shapes and temperature-dependent properties. Entropy 2018;20:118. https://doi.org/10.3390/e20020118.
[4] A.F. Ioffe-Semiconductor Thermoelements and Thermoelectric Cooling -Infosearch (1957)_text.pdf n.d.
[5] Cherkez RG. Energy possibilities of permeable generator thermoelements based on segmented legs. Thessaloniki, Greece. 2012. p. 439–42. https://doi.org/10.1063/1.4731590.
[6] Tian M-W, Mihardjo LWW, Moria H, Asaadi S, Sadighi Dizaji H, Khalilarya S, et al. A comprehensive energy efficiency study of segmented annular thermoelectric generator; thermal, exergetic and economic analysis. Appl Therm Eng 2020;181:115996. https://doi.org/10.1016/j.applthermaleng.2020.115996.
[7] Ge Y, Lin Y, He Q, Wang W, Chen J, Huang S-M. Geometric optimization of segmented thermoelectric generators for waste heat recovery systems using genetic algorithm. Energy 2021;233:121220. https://doi.org/10.1016/j.energy.2021.121220.
[8] Chen W-H, Chiou Y-B. Geometry design for maximizing output power of segmented skutterudite thermoelectric generator by evolutionary computation. Appl Energy 2020;274:115296. https://doi.org/10.1016/j.apenergy.2020.115296.
[9] Wen ZF, Sun Y, Zhang AB, Wang BL, Wang J, Du JK. Performance analysis of a segmented annular thermoelectric generator. J Electron Mater 2020;49:4830–42. https://doi.org/10.1007/s11664-020-08208-5.
[10] Aljaghtham M, Celik E. Numerical analysis of energy conversion efficiency and thermal reliability of novel, unileg segmented thermoelectric generation systems. Int J Energy Res 2021;45:8810–23. https://doi.org/10.1002/er.6416.
[11] Ahmadi Atouei S, Ranjbar AA, Rezania A. Experimental investigation of two-stage thermoelectric generator system integrated with phase change materials. Appl Energy 2017;208:332–43. https://doi.org/10.1016/j.apenergy.2017.10.032.
[12] Asaadi S, Khalilarya S, Jafarmadar S. A thermodynamic and exergoeconomic numerical study of two-stage annular thermoelectric generator. Appl Therm Eng 2019;156:371–81. https://doi.org/10.1016/j.applthermaleng.2019.04.058.
[13] Sun H, Ge Y, Liu W, Liu Z. Geometric optimization of two-stage thermoelectric generator using genetic algorithms and thermodynamic analysis. Energy 2019;171:37–48. https://doi.org/10.1016/j.energy.2019.01.003.
[14] Yin T, Li W-T, Li K, He Z-Z. Multi-parameter optimization and uncertainty analysis of multi-stage thermoelectric generator with temperature-dependent materials. Energy Rep 2021;7:7212–23. https://doi.org/10.1016/j.egyr.2021.10.079.
[15] Zhang F, Cheng L, Wu M, Xu X, Wang P, Liu Z. Performance analysis of two-stage thermoelectric generator model based on Latin hypercube sampling. Energ Conver Manage 2020;221:113159. https://doi.org/10.1016/j.enconman.2020.113159.
[16] Guo X, Zhang H, Wang J, Zhao J, Wang F, Miao H, et al. A new hybrid system composed of high-temperature proton exchange fuel cell and two-stage thermoelectric generator with Thomson effect: energy and exergy analyses. Energy 2020;195:117000. https://doi.org/10.1016/j.energy.2020.117000.

[17] Chen X, Huang Y, Chen Z. Energy and exergy analysis of an integrated photovoltaic module and two-stage thermoelectric generator system. Appl Therm Eng 2022;212:118605. https://doi.org/10.1016/j.applthermaleng.2022.118605.
[18] Sahoo RR, Karana DR. Effect of design shape factor on exergonic performance of a new modified extended-tapering segmented thermoelectric generator system. Energy 2020;200:117561. https://doi.org/10.1016/j.energy.2020.117561.
[19] Raihan Mohammad Siddique A, Kratz F, Mahmud S, Van Heyst B. Energy conversion by nanomaterial-based trapezoidal-shaped leg of thermoelectric generator considering convection heat transfer effect. J Energy Resour Technol 2019;141:082001. https://doi.org/10.1115/1.4042644.
[20] Bian M, Xu Z, Meng C, Zhao H, Tang X. Novel geometric design of thermoelectric leg based on 3D printing for radioisotope thermoelectric generator. Appl Therm Eng 2022;212:118514. https://doi.org/10.1016/j.applthermaleng.2022.118514.
[21] Mohammad Siddique AR, Mahmud S, Van Heyst B. Performance comparison between rectangular and trapezoidal-shaped thermoelectric legs manufactured by a dispenser printing technique. Energy 2020;196:117089. https://doi.org/10.1016/j.energy.2020.117089.
[22] Weng Z, Liu F, Zhu W, Li Y, Xie C, Deng J, et al. Performance improvement of variable-angle annular thermoelectric generators considering different boundary conditions. Appl Energy 2022;306:118005. https://doi.org/10.1016/j.apenergy.2021.118005.
[23] Li M, Dizaji HS, Asaadi S, Jarad F, Anqi AE, Wae-hayee M. Thermo-economic, exergetic and mechanical analysis of thermoelectric generator with hollow leg structure; impact of leg cross-section shape and hollow-to-filled area ratio. Case Stud Therm Eng 2021;27:101314. https://doi.org/10.1016/j.csite.2021.101314.
[24] Zhu Y, Newbrook DW, Dai P, Liu J, de Groot CHK, Huang R. Segmented thermoelectric generator modelling and optimization using artificial neural networks by iterative training. Energy AI 2023;12:100225. https://doi.org/10.1016/j.egyai.2022.100225.
[25] Pang D, Zhang A. Performance analysis of an annular thermoelectric generator considering Thomson effect and convection heat transfer at cold junction. J. Renew. Sustain. Energy 2020;12:064701. https://doi.org/10.1063/5.0024430.
[26] Maduabuchi C. Improving the performance of a solar thermoelectric generator using nano-enhanced variable area pins. Appl Therm Eng 2022;206:118086. https://doi.org/10.1016/j.applthermaleng.2022.118086.
[27] Tian L, Chen L, Ge Y, Shi S. Maximum efficient power performance analysis and multi-objective optimization of two-stage thermoelectric generators. Entropy 2022;24:1443. https://doi.org/10.3390/e24101443.
[28] Ajah SA, Ezurike BO, Njoku HO, Ajah SA, Ezurike BO, Njoku HO. A comparative study of energy and exergy performances of a PCM-augmented cement and fired-brick Trombe wall systems cement and fired-brick Trombe wall systems article history. Int J Ambient Energy 2020;0:1–17. https://doi.org/10.1080/01430750.2020.1718753.
[29] Petela R. Exergy of heat radiation. J Heat Transfer 1964;86:187–92. https://doi.org/10.1115/1.3687092.
[30] Majeau-Bettez G, Hawkins TR, Strømman AH. Life cycle environmental assessment of lithium-ion and nickel metal hydride batteries for plug-in hybrid and battery electric vehicles. Environ Sci Technol 2011;45:4548–54. https://doi.org/10.1021/es103607c.
[31] Carbon Footprint of Electricity Generation. https://www.parliament.uk/globalassets/documents/post/postpn268.pdf; 2023 (accessed May 23, 2023).
[32] Dubai climate: Weather by month, temperature, precipitation, when to go. https://www.climatestotravel.com/climate/united-arab-emirates/dubai; 2023 (accessed May 25, 2023).
[33] Yee SK, LeBlanc S, Goodson KE, Dames C. $ per W metrics for thermoelectric power generation: beyond ZT. Energ Environ Sci 2013;6:2561–71. https://doi.org/10.1039/C3EE41504J.
[34] Tian M-W, Mihardjo LWW, Moria H, Asaadi S, Pourhedayat S, Sadighi Dizaji H, et al. Economy, energy, exergy and mechanical study of co-axial ring shape configuration of legs as a novel structure for cylindrical thermoelectric generator. Appl Therm Eng 2021;184:116274. https://doi.org/10.1016/j.applthermaleng.2020.116274.
[35] Antonik M, O'Connor BT, Ferguson S. Performance and design comparison of a bulk thermoelectric cooler with a hybrid architecture. J Therm Sci Eng Appl 2016;8:021022. https://doi.org/10.1115/1.4032637.
[36] Cai Y, Hong B-H, Zhuang S-Q, An R-B, Wu W-X, Zhao F-Y. Numerical analysis of a solar driven thermoelectric generator brick with phase change materials: performance evaluation and parametric investigations. Appl Therm Eng 2022;214:118879. https://doi.org/10.1016/j.applthermaleng.2022.118879.
[37] Kossyvakis DN, Vossou CG, Provatidis CG, Hristoforou EV. Computational analysis and performance optimization of a solar thermoelectric generator. Renew Energy 2015;81:150–61. https://doi.org/10.1016/j.renene.2015.03.026.
[38] Kraemer D, Poudel B, Feng H-P, Caylor JC, Yu B, Yan X, et al. High-performance flat-panel solar thermoelectric generators with high thermal concentration. Nat Mater 2011;10:532–8. https://doi.org/10.1038/nmat3013.
[39] Johansson A, Kehlet B, Larson MG, Logg A. Multimesh finite element methods: solving PDEs on multiple intersecting meshes. Comput Methods Appl Mech Eng 2019;343:672–89. https://doi.org/10.1016/j.cma.2018.09.009.